Driven Hubbard model on a triangular lattice: Tunable Heisenberg antiferromagnet with a chiral three-spin term

Samudra Sur,[1] Adithi Udupa,[1] and Diptiman Sen [1,2]

[1]*Center for High Energy Physics, Indian Institute of Science, Bengaluru 560012, India*
[2]*Department of Physics, Indian Institute of Science, Bengaluru 560012, India*

We study the effects of a periodically varying electric field on the Hubbard model at half filling on a triangular lattice. The electric field is incorporated through the phase of the nearest-neighbor hopping amplitude via the Peierls prescription. When the on-site interaction U is much larger than the hopping, the effective Hamiltonian H_{eff} describing the spin sector can be found using a Floquet perturbation theory. To third order in the hopping, H_{eff} is found to have the form of a Heisenberg antiferromagnet with three different nearest-neighbor couplings $(J_\alpha, J_\beta, J_\gamma)$ on bonds lying along the different directions. Remarkably, when the periodic driving does not have time-reversal symmetry, H_{eff} can also have a chiral three-spin interaction in each triangle, with the coefficient C of the interaction having opposite signs on up- and down-pointing triangles. Thus periodic driving which breaks time-reversal symmetry can simulate the effect of a perpendicular magnetic flux which is known to generate such a chiral term in the spin sector, even though our model does not have a magnetic flux. The four parameters $(J_\alpha, J_\beta, J_\gamma, C)$ depend on the amplitude, frequency, and direction of the oscillating electric field. We then study the spin model as a function of these parameters using exact diagonalization and find a rich phase diagram of the ground state with seven different phases consisting of two kinds of ordered phases (collinear and coplanar) and disordered phases. Thus periodic driving of the Hubbard model on the triangular lattice can lead to an effective spin model whose couplings can be tuned over a range of values thereby producing a variety of interesting phases.

I. INTRODUCTION

Periodically driven quantum systems have been studied extensively over the last several years, both theoretically [1–38] and experimentally [39–50] (see Refs. [51–57] for reviews). Such systems can exhibit a wide variety interesting phenomena such as dynamical freezing [1,4,7,10–12,16–18], the generation of nontrivial band structures and states localized at the boundaries of the system [58–84], and time crystals [30,32,85]. While periodic driving of systems of non-interacting electrons has been studied very extensively, the effects of interactions along with periodic driving have also been studied by several groups [12,19–38,48–50,84].

For undriven (time-independent) systems, it is often of interest to consider a subset of states such as the ground state and low-lying excitations which dominate the low-temperature properties of the system. For this purpose it is convenient to find an effective low-energy Hamiltonian H_{eff} which describes such states; the derivation of H_{eff} usually involves taking into account all the other states in a perturbative way. For a system in which the Hamiltonian changes with time, we cannot define energy eigenstates and there is no concept of low-energy states. However, as we will see, we can define an effective time-independent Hamiltonian which describes a particular sector of the system, such as the spin sector in which each site is occupied by only one electron whose spin can point up or down.

In this paper, we will consider the Hubbard model of spin-1/2 electrons on a triangular lattice with a nearest-neighbor hopping amplitude g and an on-site interaction U. In the absence of periodic driving, it is known that when the system is at half filling and $U \gg g$, then up to order g^2, the low-energy Hamiltonian takes the form of a Heisenberg antiferromagnet with nearest-neighbor interactions of the form $J\vec{S}_i \cdot \vec{S}_j$ where $J = 4g^2/U$. We will consider what happens when this model is subjected to a periodically varying electric field which points in some direction in the plane of the lattice. The effect of the electric field will be incorporated in the model using the Peierls prescription [86]. We will show that up to order g^3, the Floquet Hamiltonian which describes Floquet eigenstates in the spin sector (i.e., with large weights for states in which every site is singly occupied) has the following form. At order g^2 and g^3 there is a Heisenberg antiferromagnetic term $J_a\vec{S}_i \cdot \vec{S}_j$ which couples nearest neighbors but the coupling J_a has three different values depending on the orientation of the bond joining the two sites. In addition, if the periodically varying electric field is not time-reversal symmetric, a chiral three-spin interaction of the form $C\vec{S}_i \cdot \vec{S}_j \times \vec{S}_k$ can appear at order g^3 on each triangle, with C having *opposite* values $\pm C$ on up- and down-pointing triangles. The values of the four couplings, J_a and C, can be tuned by varying the time dependence and direction of the periodically varying electric field and the driving frequency ω. A spin model with four such couplings has not been studied earlier to the best of our knowledge although

Refs. [87–90] have studied models with different values of J_a and $C = 0$, and models with all J_a's equal and C having the *same* sign on up- and down-pointing triangles have been studied in Refs. [91] and [92]. We will then study the ground state phase diagram of our four-parameter spin model using exact diagonalization (ED) of systems with 36 sites. We find a rich phase diagram consisting of three collinear ordered phases, one coplanar ordered phase, and three disordered (spin-liquid) phases. These phases can be distinguished from each other in several ways including the locations of the peaks of the static spin structure function $S(\vec{q})$ in the Brillouin zone of $\vec{q}$, the minimum value of the correlation function $C(\vec{r})$ in real space, the fidelity susceptibility of the ground state [93], and crossings of the energies of the ground state and first excited state.

The plan of the paper is as follows. In Sec. II we introduce the Hubbard model on a triangular lattice in the presence of a periodically varying electric field. In Sec. III we derive the effective spin Hamiltonian using a Floquet perturbation theory which works in the limit that the nearest-neighbor hopping is much smaller than the Hubbard interaction U and the driving frequency ω. We will find that there are nearest-neighbor Heisenberg antiferromagnetic terms with three different couplings $J_\alpha, J_\beta, J_\gamma$ and a chiral three-spin term with coefficient $\pm C$ on up- and down-pointing triangles. In Sec. IV, we study the ground state phase diagram of the effective Floquet Hamiltonian in the classical limit and then use spin-wave theory to look at the excitations in the collinear phases. This is followed by Sec. V in which we study the spin model in detail using ED for various values of J_α, J_β, J_γ, and C. We look at several quantities derived from the ground state wave function such as the static structure function in both real and momentum space and the fidelity susceptibility to obtain the ground state phase diagram. A rich phase diagram is found with four ordered phases and three spin-liquid phases. We conclude in Sec. VI by summarizing our main results and pointing out possible directions for future studies.

II. HUBBARD MODEL WITH PERIODIC DRIVING BY ELECTRIC FIELD

We consider the one-band Hubbard model of spin-1/2 electrons on a triangular lattice at half filling. The Hamiltonian is given by

$$H = -g \sum_{\langle i,j \rangle, \sigma} (c_{i,\sigma}^\dagger c_{j,\sigma} + \text{H.c.}) + U \sum_i n_{i,\uparrow} n_{i,\downarrow}, \quad (1)$$

where g is the hopping amplitude between neighboring sites, and $U > 0$ is the on-site repulsive interaction. In the absence of driving and in the limit of large interaction, $U \gg g$, the lowest energy sector of the Hamiltonian is described by an antiferromagnetic Heisenberg spin model at half filling and by the t-J model away from half filling. Additionally, we drive the Hamiltonian periodically with a time varying in-plane electric field $\vec{E}(\vec{r}, t) = \vec{E}(\vec{r}, t + T)$. To consider the most general cases, we will assume that the electric field is *not* time-reversal symmetric, i.e., that there is no t_0 such that $\vec{E}(\vec{r}, t) = \vec{E}(\vec{r}, t_0 - t)$. This property of the electric field will turn out to be important for our study since, as we will see, it gives rise to an additional term in the effective spin
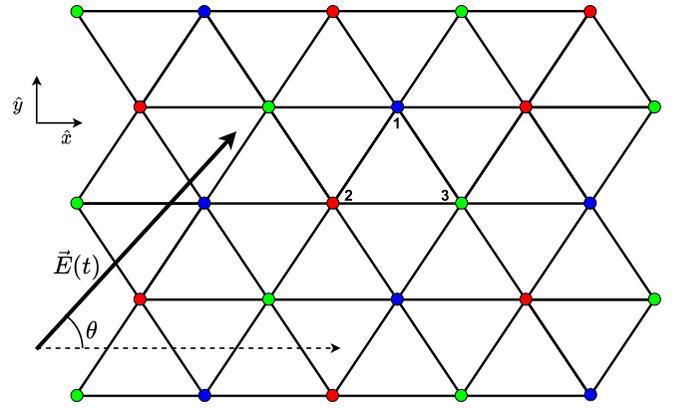
FIG. 1. A schematic of the triangular lattice model with the sublattices marked in three different colors. The sites are labeled in the anticlockwise direction 1, 2, and 3 as shown. The time-dependent electric field $\vec{E}(t)$ points along a direction $\hat{n}$ which makes an angle θ with the $\hat{x}$ axis.

Hamiltonian. (Such an electric field can be realized by, say, superposing two sinusoidal electric fields with different frequencies and a phase difference as we will see in Sec. V). We will take the form of the electric field to be $\vec{E}(t) = \hat{n}\mathcal{E}(t)$, where $\hat{n}$ denotes a unit vector in the plane of the triangular lattice, and we will parametrize the direction of $\hat{n}$ by an angle θ with respect to the $\hat{x}$ axis.

The time-dependent electric field is incorporated in our model through a vector potential in the phase of the nearest-neighbor hopping following the Peierls prescription. Since $\vec{E} = -(1/c)\partial \vec{A}/\partial t$, the vector potential is $\vec{A}(t) = \hat{n}\mathcal{A}(t)$ where $\mathcal{A}(t) = -c \int_0^t dt' \mathcal{E}(t')$. [We will assume that the electric field does not have a dc component, i.e., $\int_0^T dt\, \mathcal{E}(t) = 0$. Then $\mathcal{A}(t)$ will also be a periodic function of t.] The phase of the hopping from a site at $\vec{r}_j$ to a site at $\vec{r}_i$ is given by $(q/\hbar c)\vec{A} \cdot (\vec{r}_i - \vec{r}_j)$ where q is the charge of the electron. Hence the periodic driving modifies the term $-g c_{i,\sigma}^\dagger c_{j,\sigma}$ in the Hamiltonian to $-g e^{i(q/\hbar c)\mathcal{A}(t)\hat{n} \cdot (\vec{r}_i - \vec{r}_j)} c_{i,\sigma}^\dagger c_{j,\sigma}$.

Figure 1 illustrates how the different quantities look for a single triangle with sides of unit length whose sites are labeled as 1, 2, and 3. (We have chosen the triangle to be up-pointing along the $\hat{y}$ axis.) If t_{ij} is the hopping amplitude from site j to site i, we have

$$\begin{aligned} t_{12} &= g\, e^{i(q/\hbar c)\mathcal{A}(t)\cos(\pi/3-\theta)}, \\ t_{23} &= g\, e^{i(q/\hbar c)\mathcal{A}(t)\cos(\pi-\theta)}, \\ t_{31} &= g\, e^{i(q/\hbar c)\mathcal{A}(t)\cos(\pi/3+\theta)}, \end{aligned} \quad (2)$$

and $t_{ji} = t_{ij}^*$. Then the periodically driven Hamiltonian for this triangle is

$$H_\triangle(t) = -\sum_\sigma (t_{12} c_{1,\sigma}^\dagger c_{2,\sigma} + t_{23} c_{2,\sigma}^\dagger c_{3,\sigma} + t_{31} c_{3,\sigma}^\dagger c_{1,\sigma} + \text{H.c.})$$

$$+ U \sum_{i=1}^3 n_{i,\uparrow} n_{i,\downarrow}. \quad (3)$$

To obtain the Hamiltonian for the entire triangular lattice, we sum up the Hamiltonians for all triangles, both up-pointing
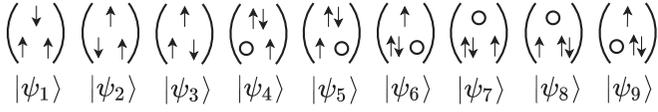
FIG. 2. The nine basis states in sector (b) are labeled from $|\psi_1\rangle$ to $|\psi_9\rangle$ as shown.

and down-pointing, with Hamiltonians $H_\triangle(t)$ and $H_\nabla(t)$. In the next section we will use Floquet perturbation theory to derive the effective model in the large U (Mott insulator) limit of this driven model. We shall see that the states in the spin sector (in which all sites are occupied by only one electron) are governed by a Heisenberg Hamiltonian with different exchange couplings on different bonds and an additional chiral three-spin term whose sign is opposite for up-pointing ($\triangle$) and down-pointing triangles (∇).

III. OBTAINING THE EFFECTIVE SPIN HAMILTONIAN USING FLOQUET PERTURBATION THEORY

To obtain the effective Hamiltonian in the large U limit using Floquet perturbation theory, we start with the Hubbard model on a single triangle. We write the Hamiltonian in Eq. (3) as $H_\triangle = H_0 + V$ where

$$H_0 = U \sum_{i=1}^{3} n_{i,\uparrow} n_{i,\downarrow},$$

$$V(t) = -\sum_\sigma (t_{12} c_{1,\sigma}^\dagger c_{2,\sigma} + t_{23} c_{2,\sigma}^\dagger c_{3,\sigma} + t_{31} c_{3,\sigma}^\dagger c_{1,\sigma} + \text{H.c.}).$$

We now consider the eigenstates of the static part of the Hamiltonian, H_0, which will serve as the basis for subsequent calculations. For a half-filled system we can have three electrons on the triangle. Then the total number of basis states is 20. They can be classified according to the number of up and down spins (in S_z basis) which are listed below:

(a) One state with all three spins pointing up.

(b) Nine states with two up spins and a down spin. Six of these states have a double occupancy.

(c) Nine states with one up and two down spins. Here also six states have a double occupancy.

(d) One state with all the three spins pointing down.

The reason for this classification is that these four sectors do not mix with each other since they have different values of the z component of the total spin S^z, which commutes with both H_0 and $V(t)$.

Sectors (a) and (d) are identical in terms of the eigenvalues of H_0 as are the sectors (b) and (c). Since the states in sector (a) and (d) are exact eigenstates of $V(t)$, the nontrivial eigenstates of H_0 are governed by states in sectors (b) and (c) which are related by the spin rotation operator which takes $S^z \rightarrow -S^z$. Hence we will derive the effective Hamiltonian for only sector (b). The nine basis states $|\psi_n\rangle$ in sector (b) are labeled as shown in Fig. 2. A general state $|\psi(t)\rangle$ with two up spins and one down spin can be written as a linear combination of these basis states as $|\psi(t)\rangle = \sum_{n=1}^{9} c_n(t) |\psi_n\rangle\, e^{-iE_n t}$, where E_n's are the eigenvalues of H_0. (We will set $\hbar$ equal to 1 in the rest of this paper.) According to our notation $E_1 = E_2 = E_3 = 0$ and $E_n = U$ for $n = 4, 5, \ldots, 9$. We will follow the

convention of defining the basis states in terms of the creation operators as follows. In Fig. 2, the state $|\psi_1\rangle = c_{1\downarrow}^\dagger c_{2\uparrow}^\dagger c_{3\uparrow}^\dagger |0\rangle$, whereas $|\psi_4\rangle = c_{1\uparrow}^\dagger c_{1\downarrow}^\dagger c_{3\uparrow}^\dagger |0\rangle$, namely, the three site labels are nondecreasing as we go from left to right, and at the same site, $\uparrow$ appears to the left of $\downarrow$.

Next, $|\psi(t)\rangle$ satisfies the time-dependent Schrödinger equation $i\partial |\psi(t)\rangle / \partial t = (H_0 + V(t)) |\psi(t)\rangle$. Using the expansion of $|\psi(t)\rangle$, we obtain a set of linear differential equations for the coefficients c_n,

$$i\frac{dc_n}{dt} = \sum_{m=1}^{9} \langle \psi_n| V(t) |\psi_m\rangle\, e^{i(E_n - E_m)t}\, c_m(t), \quad (4)$$

where $n = 1, 2, \ldots, 9$. In our chosen basis, the matrix $\langle \psi_n| V(t) |\psi_m\rangle$ matrix looks like

$$\begin{pmatrix}
0 & 0 & 0 & t_{21} & -t_{31} & 0 & t_{12} & -t_{13} & 0 \\
0 & 0 & 0 & -t_{21} & 0 & t_{32} & -t_{12} & 0 & t_{32} \\
0 & 0 & 0 & 0 & t_{31} & -t_{32} & 0 & t_{13} & -t_{23} \\
t_{12} & -t_{12} & 0 & 0 & -t_{32} & 0 & 0 & 0 & t_{13} \\
-t_{13} & 0 & t_{13} & -t_{23} & 0 & t_{12} & 0 & 0 & 0 \\
0 & t_{23} & -t_{23} & 0 & t_{21} & 0 & -t_{13} & 0 & 0 \\
t_{21} & -t_{21} & 0 & 0 & 0 & -t_{31} & 0 & t_{23} & 0 \\
-t_{31} & 0 & t_{31} & 0 & 0 & 0 & t_{32} & 0 & -t_{21} \\
0 & t_{32} & -t_{32} & t_{31} & 0 & 0 & 0 & -t_{12} & 0
\end{pmatrix}. \quad (5)$$

Since the t_{ij}'s are periodic functions of time, they can be expanded as a Fourier series. The expressions for the time-dependent hoppings are therefore

$$t_{12} = g \sum_{m=-\infty}^{\infty} \gamma_m e^{im\omega t},$$

$$t_{23} = g \sum_{m=-\infty}^{\infty} \alpha_m e^{im\omega t},$$

$$t_{31} = g \sum_{m=-\infty}^{\infty} \beta_m e^{im\omega t}, \quad (6)$$

where α_m, β_m, and γ_m are generally complex.

In Floquet theory, we define a Floquet operator which unitarily evolves the system through one time period T as

$$U_T = \mathcal{T} e^{-(i/\hbar)\int_0^T dt H(t)}, \quad (7)$$

where $\mathcal{T}$ denotes time ordering. If $|\psi(t)\rangle$ is an eigenstate of U_T, we have

$$|\psi(T)\rangle = U_T |\psi(0)\rangle = e^{-i\epsilon T} |\psi(0)\rangle, \quad (8)$$

where ϵ is the quasienergy for the state $|\psi(t)\rangle$. Then in terms of the basis states $|\psi_n\rangle$ and coefficients $c_n(t)$, we have

$$c_n(T)\, e^{-iE_n T} = \sum_{m=1}^{9} \langle \psi_n| U_T |\psi_m\rangle\, c_m(0) \quad (9)$$

for $n = 1, 2, \ldots, 9$. In the following subsections, we will solve Eq. (4) perturbatively in powers of g to obtain an effective Hamiltonian H_{eff} such that $e^{-iH_{\text{eff}}T} = U_T$ up to the desired power of g.

A. Second-order calculation for effective Hamiltonian

Starting from Eq. (4) we solve for the coefficients of the low-energy states $c_1(T)$, $c_2(T)$, $c_3(T)$ up to order g^2 perturbatively. To begin with, the equations for $c_4(t) \ldots c_9(t)$ are solved at an arbitrary time t assuming the coefficients $c_1(t)$, $c_2(t)$, $c_3(t)$ to be constant and given by their values at $t = 0$. This is because $c_4(t) \ldots c_9(t)$ are coefficients of the states $|\psi_4\rangle \ldots |\psi_9\rangle$ which lie in the high-energy sector and thus appear with coefficients which are of order g times the coefficients of $c_1(t)$, $c_2(t)$, $c_3(t)$. This procedure gives equations of the form

$$c_4(t) - c_4(0) = -g \sum_m \gamma_m \frac{(e^{i(U+m\omega)t} - 1)}{U + m\omega} c_1(0)$$
$$+ g \sum_m \gamma_m \frac{(e^{i(U+m\omega)t} - 1)}{U + m\omega} c_2(0) \quad (10)$$

and similar equations for $c_5(t) \ldots c_9(t)$. We now have to impose the Floquet condition Eq. (8) for the coefficients. We have $c_4(T) = e^{-i\epsilon T} e^{iUT} c_4(0)$. The Floquet eigenvalue $e^{-i\epsilon T}$ gives the amplitude $\langle \psi(T) | \psi(0) \rangle$, which is the amplitude to start at time $t = 0$ with a combination of the nine basis states and come back to the same combination of states (up to overall phase) at time $t = T$. However this is either an order 1 or order g^2 process. This allows us to approximate $e^{-i\epsilon T} = \mathbb{1} + O(g^2)$. Hence, up to first order in g, we can write

$$c_4(T) - c_4(0) = (e^{iUT} - 1) c_4(0). \quad (11)$$

Using this Floquet condition at $t = T$ in Eq. (10) we obtain the order g expression for c_4

$$c_4(t) = -g \sum_m \gamma_m \frac{e^{i(U+m\omega)t}}{U + m\omega} c_1(0)$$
$$+ g \sum_m \gamma_m \frac{e^{i(U+m\omega)t}}{U + m\omega} c_2(0). \quad (12)$$

We get similar expressions for the coefficients $c_5(t) \ldots c_9(t)$.

In the next step we substitute these $O(g)$ expressions for $c_4(t) \ldots c_9(t)$ in the right hand side of Eq. (4) to obtain the $O(g^2)$ equations for $c_1(T)$, $c_2(T)$, $c_3(T)$, which eventually gives the second-order effective Hamiltonian for the Floquet system. We can write down final equations in a matrix form,

$$\begin{pmatrix} c_1(T) \\ c_2(T) \\ c_3(T) \end{pmatrix} = (\mathbb{1} - iT H_{\text{eff}}^{(2)}) \begin{pmatrix} c_1(0) \\ c_2(0) \\ c_3(0) \end{pmatrix}, \quad (13)$$

where

$$H_{\text{eff}}^{(2)} = g^2 \begin{pmatrix} -f_\beta - f_\gamma & f_\gamma & f_\beta \\ f_\gamma & -f_\alpha - f_\gamma & f_\alpha \\ f_\beta & f_\alpha & -f_\alpha - f_\beta \end{pmatrix},$$

$$f_\alpha = \sum_m |\alpha_m^2| \left(\frac{1}{U + m\omega} + \frac{1}{U - m\omega} \right),$$

$$f_\beta = \sum_m |\beta_m^2| \left(\frac{1}{U + m\omega} + \frac{1}{U - m\omega} \right),$$

$$f_\gamma = \sum_m |\gamma_m^2| \left(\frac{1}{U + m\omega} + \frac{1}{U - m\omega} \right). \quad (14)$$

Comparing with Eq. (9) and noting that $E_1 = E_2 = E_3 = 0$, we infer that $(\mathbb{1} - iT H_{\text{eff}}^{(2)})$ approximates U_T to $O(g^2)$.

We note that the quantities in Eq. (14) diverge if U/ω approaches any integer values. This corresponds to a resonance condition, and the coefficients $c_4(t) \ldots c_9(t)$ of the high-energy states will then not be much smaller than $c_1(t)$, $c_2(t)$, $c_3(t)$. In our numerical calculations, we will choose U and ω in such a way that U/ω is not close to an integer.

B. Third-order calculation for effective Hamiltonian

The third-order effective Hamiltonian is obtained by solving for $c_1(T)$, $c_2(T)$, $c_3(T)$ to $O(g^3)$. Here we start with the $O(g)$ expressions for $c_4(t) \ldots c_9(t)$ which have already been calculated in Eq. (12). We now use these expressions in the right hand side of the equations involving $c_4(t) \ldots c_9(t)$ in Eq. (4) to find the same expressions to the next order in g. We again use the Floquet condition to finally end up with the $O(g^2)$ expressions for $c_4(t) \ldots c_9(t)$. The final expression for $c_4(t)$ in Eq. (15) is given by

$$c_4(t) = -g^2 \sum_{m,n} \frac{\alpha_n^* \beta_m^* e^{i(U-m\omega-n\omega)t}}{(U - m\omega)(U - m\omega - n\omega)} (c_1(0) - c_3(0))$$
$$+ g^2 \sum_{m,n} \frac{\alpha_m^* \beta_n^* e^{i(U-m\omega-n\omega)t}}{(U - m\omega)(U - m\omega - n\omega)} (c_2(0) - c_3(0)). \quad (15)$$

Next, we use this expression along with similar expressions for $c_5(t) \ldots c_9(t)$ in the right hand side of Eq. (4) which finally gives us $O(g^3)$ expressions for $c_1(T)$, $c_2(T)$, $c_3(T)$. The third-order effective Hamiltonian $H_{\text{eff}}^{(3)}$ obtained from this calculation is given by

$$H_{\text{eff}}^{(3)} = g^3 \begin{pmatrix} (d_\alpha + d_\alpha^*) - (e_\alpha + e_\alpha^*) & (e_\alpha^* + e_\beta^* + d_\gamma^*) - (d_\alpha + d_\beta + e_\gamma) & (e_\alpha + d_\beta + e_\gamma) - (d_\alpha^* + e_\beta^* + d_\gamma^*) \\ (e_\alpha + e_\beta + d_\gamma) - (d_\alpha^* + d_\beta^* + e_\gamma^*) & (d_\beta + d_\beta^*) - (e_\beta + e_\beta^*) & (d_\alpha^* + e_\beta^* + e_\gamma^*) - (e_\alpha + d_\beta + d_\gamma) \\ (e_\alpha^* + d_\beta^* + e_\gamma^*) - (d_\alpha + e_\beta + d_\gamma) & (d_\alpha + e_\beta + e_\gamma) - (e_\alpha^* + d_\beta^* + d_\gamma^*) & (d_\gamma + d_\gamma^*) - (e_\gamma + e_\gamma^*) \end{pmatrix}, \quad (16)$$

where we define

$$d_\alpha = \sum_{l,m} \frac{\alpha_{-(l+m)} \beta_m \gamma_l}{(U - m\omega)(U + l\omega)},$$

$$d_\beta = \sum_{l,m} \frac{\beta_{-(l+m)} \gamma_m \alpha_l}{(U - m\omega)(U + l\omega)},$$

$$d_\gamma = \sum_{l,m} \frac{\gamma_{-(l+m)} \alpha_m \beta_l}{(U - m\omega)(U + l\omega)},$$

$$e_\alpha = \sum_{l,m} \frac{\alpha_{-(l+m)} \, \beta_m \, \gamma_l}{(U + m\omega)(U - l\omega)},$$

$$e_\beta = \sum_{l,m} \frac{\beta_{-(l+m)} \, \gamma_m \, \alpha_l}{(U + m\omega)(U - l\omega)},$$

$$e_\gamma = \sum_{l,m} \frac{\gamma_{-(l+m)} \, \alpha_m \, \beta_l}{(U + m\omega)(U - l\omega)}. \tag{17}$$

Thus, by considering the lowest energy states for a single triangle pointing upwards, we obtain the effective Hamiltonian for this driven system $H_\triangle^{\rm eff} = H_{\rm eff}^{(2)} + H_{\rm eff}^{(3)}$ up to $O(g^3)$. We can now rewrite this Hamiltonian in terms of spin operators at the three sites. Our original Hamiltonian Eq. (1), as

well as the driven Hamiltonian Eq. (3) are $SU(2)$ invariant, hence the effective Hamiltonian will also have the same spin rotational symmetry. The form of our Hamiltonian for three spin-1/2's on a triangle can therefore have only the following terms,

$$H_\triangle^{\rm eff} = J_\alpha \, \vec{S}_2 \cdot \vec{S}_3 \, + \, J_\beta \, \vec{S}_3 \cdot \vec{S}_1 \, + \, J_\gamma \, \vec{S}_1 \cdot \vec{S}_2$$
$$+ \, C \, \vec{S}_1 \cdot \vec{S}_2 \times \vec{S}_3 \, + \, D \, \mathbb{1}, \tag{18}$$

where J_α, J_β, J_γ are the two-spin exchange couplings, C is a chiral three-spin term, and D is a constant. In the basis states of sector (b), $(|\psi_1\rangle, |\psi_2\rangle, |\psi_3\rangle)$, at sites 1, 2, and 3, this Hamiltonian has the following form:

$$H_\triangle^{\rm eff} \begin{pmatrix} |\psi_1\rangle \\ |\psi_2\rangle \\ |\psi_3\rangle \end{pmatrix} = \begin{pmatrix} \frac{1}{4}(J_\alpha - J_\beta - J_\gamma) + D & \frac{1}{2}J_\gamma + \frac{i}{4}C & \frac{1}{2}J_\beta - \frac{i}{4}C \\ \frac{1}{2}J_\gamma - \frac{i}{4}C & \frac{1}{4}(J_\beta - J_\alpha - J_\gamma) + D & \frac{1}{2}J_\alpha + \frac{i}{4}C \\ \frac{1}{2}J_\beta + \frac{i}{4}C & \frac{1}{2}J_\alpha - \frac{i}{4}C & \frac{1}{4}(J_\gamma - J_\alpha - J_\beta) + D \end{pmatrix} \begin{pmatrix} |\psi_1\rangle \\ |\psi_2\rangle \\ |\psi_3\rangle \end{pmatrix}. \tag{19}$$

Comparing this equation with Eq. (18), we obtain expressions for J_α, J_β, J_γ, and C. We further obtain the expression for D using the special state of sector (a) with all three spins pointing up. This state has an eigenvalue equal to $\frac{1}{4}(J_\alpha + J_\beta + J_\gamma) + D$ for the Hamiltonian in Eq. (18). But for our original Hamiltonian, this gives an energy eigenvalue equal to zero. Equating the two, we obtain D. The expressions for the five parameters are therefore given by

$$J_\alpha = 2g^2 f_\alpha \, - \, 2g^3 \, {\rm Re}\,[(d_\alpha + e_\beta + e_\gamma) - (e_\alpha + d_\beta + d_\gamma)],$$

$$J_\beta = 2g^2 f_\beta \, - \, 2g^3 \, {\rm Re}\,[(e_\alpha + d_\beta + e_\gamma) - (d_\alpha + e_\beta + d_\gamma)],$$

$$J_\gamma = 2g^2 f_\gamma \, - \, 2g^3 \, {\rm Re}\,[(e_\alpha + e_\beta + d_\gamma) - (d_\alpha + d_\beta + e_\gamma)],$$

$$C = -4g^3 \, {\rm Im}\,[d_\alpha + d_\beta + d_\gamma + e_\alpha + e_\beta + e_\gamma],$$

$$D = -\frac{1}{4}(J_\alpha + J_\beta + J_\gamma). \tag{20}$$

Interestingly, we observe that C is zero when the d's and e's defined in Eq. (17) are real. This is the case if the Hamiltonian is time-reversal symmetric, i.e., $H(t_0 - t) = H^*(t)$ for some value of t_0. Then the Fourier expansions for the time-dependent hoppings obey $\sum_{m=-\infty}^{\infty} \alpha_m \, e^{im\omega(t_0-t)} = \sum_{m=-\infty}^{\infty} \alpha_m^* \, e^{-im\omega t}$. This implies that $\alpha_m^* = \alpha_m \, e^{im\omega t_0}$ for all m and similarly for β_m's and γ_m's. This makes the d's and e's defined in Eq. (17) completely real.

However, for circularly polarized radiation where the vector potential is of the form $\vec{A}(t) = A[\cos(\omega t)\hat{x} + \sin(\omega t)\hat{y}]$, time-reversal symmetry is broken, but we find from Eqs. (2) and (20) that C vanishes at order g^3 for all values of A and ω. (It turns out that we get a nonzero contribution to C at order g^4 as shown in Refs. [94–96].) Thus breaking time-reversal symmetry is a necessary but not sufficient condition to have a nonzero C at order g^3.

The expressions for the second-order and third-order effective Hamiltonians in Eqs. (14) and (16) indicate that the perturbative expansion is valid if g is much smaller than U, ω

and $U + n\omega$ for any integer value of n. The condition that g should be much smaller than $U + n\omega$ for any n is required to avoid resonances.

C. Total effective Hamiltonian for the lattice

The effective Hamiltonian for a single up-pointing triangle, as derived above in the spin operator language, can be extended to the entire lattice. The important observation to note here is that the coefficient of the chiral three-spin term written in the the anticlockwise direction is opposite on up- and down-pointing triangles. (This is unlike the case of a time-independent magnetic field applied perpendicular to the plane of the lattice which gives the same sign of the chiral term for all triangles, both up- and down-pointing. This is because the chiral three-spin term then only depends on the magnetic flux through each triangle, and this has the same sign for all triangles [97].) The reason for the sign flip in our model is that when we go from $\triangle \rightarrow \triangledown$, the angle that the external electric field makes with $\hat{x}$ changes as $\theta \rightarrow \pi + \theta$. This changes the hoppings as $t_{ij} \rightarrow t_{ij}^*$ and thus, $d_k, e_k \rightarrow d_k^*, e_k^*$. From Eq. (20) we see that this gives a negative sign on the right hand side in the expression for C. Hence $C \rightarrow -C$ when we go from an $\triangle$ triangle to a $\triangledown$ triangle.

The complete triangular lattice is made up of up-pointing and down-pointing triangles placed adjacently to each other. The total Hamiltonian for the lattice in the spin operator language can thus be written as

$$H_L = \sum_{\vec{n}} [J_\alpha \vec{S}_{\vec{n}} \cdot \vec{S}_{\vec{n}+\vec{u}} + J_\beta \vec{S}_{\vec{n}} \cdot \vec{S}_{\vec{n}+\vec{v}} + J_\gamma \vec{S}_{\vec{n}} \cdot \vec{S}_{\vec{n}+\vec{w}}]$$

$$+ C \Bigg[\sum_{\vec{n},\triangle} \vec{S}_{\vec{n}} \cdot \vec{S}_{\vec{n}+\vec{u}} \times \vec{S}_{\vec{n}+\vec{w}}$$

$$- \sum_{\vec{n},\triangledown} \vec{S}_{\vec{n}} \cdot \vec{S}_{\vec{n}+\vec{w}} \times \vec{S}_{\vec{n}+\vec{v}} \Bigg], \tag{21}$$
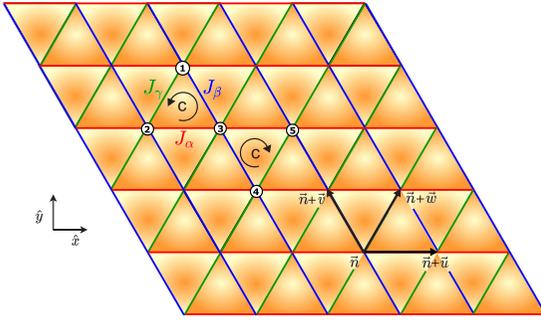
FIG. 3. A schematic of the triangular lattice model with the nearest-neighbor position vectors $\vec{u}$, $\vec{v}$, and $\vec{w}$ and effective Heisenberg couplings J_α, J_β, and J_γ for three different bonds as shown. The chiral three-spin term has opposite signs of C for up-pointing (123) and down-pointing (345) triangles.

where $\vec{n} = m_1\vec{u} + m_2\vec{v}$ is the vector position of a site on the lattice, and

$$\vec{u} = a\hat{x},$$
$$\vec{v} = a\left(-\frac{1}{2}\hat{x} + \frac{\sqrt{3}}{2}\hat{y}\right),$$
$$\vec{w} = a\left(\frac{1}{2}\hat{x} + \frac{\sqrt{3}}{2}\hat{y}\right) \qquad (22)$$

as shown in Fig. 3. (We will henceforth set the nearest-neighbor lattice spacing $a = 1$.) The order of spin operators for the three-spin terms is conventionally taken to be in the anticlockwise direction. This convention gives a negative sign for C for the down-pointing triangle. For instance, in Fig. 3, the three-spin term for the down-pointing triangle marked by sites 3, 4, and 5 is $-C\,\vec{S}_3 \cdot \vec{S}_4 \times \vec{S}_5$.

IV. CLASSICAL ANALYSIS AND SPIN-WAVE THEORY

In this section we will consider the spin-1/2 Hamiltonian on the triangular lattice and study its classical limit where the value of the spin S at each site is taken to infinity. Having found the classical ground state we will then use spin-wave theory to study the excitations above the classical ground state.

In the large-S limit, we have to put a factor of $1/S$ in front of the three-spin term so that it scales in the same way (i.e., as S^2) as the two-spin terms. We therefore consider the Hamiltonian

$$H_S = \sum_{\vec{n}}[J_\alpha\vec{S}_{\vec{n}} \cdot \vec{S}_{\vec{n}+\vec{u}} + J_\beta\vec{S}_{\vec{n}} \cdot \vec{S}_{\vec{n}+\vec{v}} + J_\gamma\vec{S}_{\vec{n}} \cdot \vec{S}_{\vec{n}+\vec{w}}]$$
$$+ \frac{C}{S}\Bigg[\sum_{\vec{n},\triangle}\vec{S}_{\vec{n}} \cdot \vec{S}_{\vec{n}+\vec{u}} \times \vec{S}_{\vec{n}+\vec{w}}$$
$$- \sum_{\vec{n},\triangledown}\vec{S}_{\vec{n}} \cdot \vec{S}_{\vec{n}+\vec{w}} \times \vec{S}_{\vec{n}+\vec{v}}\Bigg]. \qquad (23)$$

Since we are looking at the classical limit, we can take the components of spin to be commuting objects. We will now look at some classical spin configurations and find the ranges of parameters $(J_\alpha, J_\beta, J_\gamma, C)$ where each of these is stable.

Before proceeding further, we note that $\vec{w} = \vec{u} + \vec{v}$, and the coordinates $\vec{n}$ of any site can be uniquely written as

$$\vec{n} = m_1\vec{u} + m_2\vec{v}, \qquad (24)$$

where m_1, m_2 are integers.

We first consider a collinear spin configuration in which all the spins point along the $\pm\hat{z}$ direction in the spin space, and they also satisfy

$$\vec{S}_{\vec{n}} \cdot \vec{S}_{\vec{n}+\vec{u}} = -S^2,$$
$$\vec{S}_{\vec{n}} \cdot \vec{S}_{\vec{n}+\vec{v}} = S^2,$$
$$\vec{S}_{\vec{n}} \cdot \vec{S}_{\vec{n}+\vec{w}} = -S^2 \qquad (25)$$

for all values of $\vec{n}$. Following Fig. 3 and Eq. (24), we see that a spin configuration which satisfies Eq. (25) is given by

$$\vec{S}_{\vec{n}} = S(0, 0, (-1)^{m_1}). \qquad (26)$$

For a large system with N sites and periodic boundary conditions, we find that the classical energy of this configuration is given by

$$E_{cl} = NS^2(-J_\alpha + J_\beta - J_\gamma). \qquad (27)$$

[Note that the three-spin term in Eq. (23) does not contribute to the energy in any collinear spin configuration. We will therefore set $C = 0$ in the rest of this analysis.] We will now use spin-wave theory [98,99] to find the energy-momentum dispersion of the excitations around the classical ground state in Eq. (26). We use the Holstein-Primakoff transformation [100] to write the spin operators in terms of bosonic operators as

$$S_{\vec{n}}^z = S - a_{\vec{n}}^\dagger a_{\vec{n}},$$
$$S_{\vec{n}}^+ = \sqrt{2S - a_{\vec{n}}^\dagger a_{\vec{n}}}\, a_{\vec{n}}$$
$$S_{\vec{n}}^- = a_{\vec{n}}^\dagger\sqrt{2S - a_{\vec{n}}^\dagger a_{\vec{n}}} \qquad (28)$$

at the sites where $\vec{S}_{\vec{n}} = S(0, 0, 1)$, and

$$S_{\vec{n}}^z = -S + a_{\vec{n}}^\dagger a_{\vec{n}},$$
$$S_{\vec{n}}^+ = a_{\vec{n}}^\dagger\sqrt{2S - a_{\vec{n}}^\dagger a_{\vec{n}}},$$
$$S_{\vec{n}}^- = \sqrt{2S - a_{\vec{n}}^\dagger a_{\vec{n}}}\, a_{\vec{n}}, \qquad (29)$$

at the sites where $\vec{S}_{\vec{n}} = S(0, 0, -1)$. Making the standard large-S approximation of replacing $\sqrt{2S - a_{\vec{n}}^\dagger a_{\vec{n}}} \rightarrow \sqrt{2S}$, we find that Eq. (23) takes the form

$$H_S = NS^2(-J_\alpha + J_\beta - J_\gamma)$$
$$+ S\sum_{\vec{n}}[(2J_\alpha - 2J_\beta + 2J_\gamma)a_{\vec{n}}^\dagger a_{\vec{n}}$$
$$+ J_\alpha(a_{\vec{n}}^\dagger a_{\vec{n}+\vec{u}}^\dagger + \text{H.c.})$$
$$+ J_\beta(a_{\vec{n}}^\dagger a_{\vec{n}+\vec{v}} + \text{H.c.})$$
$$+ J_\gamma(a_{\vec{n}}^\dagger a_{\vec{n}+\vec{w}}^\dagger + \text{H.c.})]. \qquad (30)$$

Fourier transforming to momentum space, we obtain

$$
\begin{aligned}
H_S = {} & NS^2(-J_\alpha + J_\beta - J_\gamma) \\
& + S\sum_{\vec{k}}[(2J_\alpha - 2J_\beta + 2J_\gamma)a_{\vec{k}}^\dagger a_{\vec{k}} \\
& \quad + J_\alpha \cos(\vec{k}\cdot\vec{u})(a_{\vec{k}}^\dagger a_{-\vec{k}}^\dagger + a_{\vec{k}}a_{-\vec{k}}) \\
& \quad + 2J_\beta \cos(\vec{k}\cdot\vec{v})a_{\vec{k}}^\dagger a_{\vec{k}} \\
& \quad + J_\gamma \cos(\vec{k}\cdot\vec{w})(a_{\vec{k}}^\dagger a_{-\vec{k}}^\dagger + a_{\vec{k}}a_{-\vec{k}})],
\end{aligned} \tag{31}
$$

where the sum over $\vec{k}$ runs over the complete Brillouin zone. The above Hamiltonian couples modes at $\vec{k}$ and $-\vec{k}$. Using the Bogoliubov transformation to diagonalize the Hamiltonian, we find that the spin-wave spectrum is given by

$$
\begin{aligned}
E_{\vec{k}} &= S\sqrt{(C_{\vec{k}} + D_{\vec{k}})(C_{\vec{k}} - D_{\vec{k}})}, \\
C_{\vec{k}} &= J_\alpha + J_\gamma - J_\beta + J_\beta \cos(\vec{k}\cdot\vec{v}), \\
D_{\vec{k}} &= J_\alpha \cos(\vec{k}\cdot\vec{u}) + J_\gamma \cos(\vec{k}\cdot\vec{w}).
\end{aligned} \tag{32}
$$

We see that the spin-wave energy vanishes at $\vec{k} = (0,0)$ and $\vec{k} = \pi(1, 1/\sqrt{3})$ which correspond to Goldstone modes. We therefore expect that in this phase the static structure function $S(\vec{q})$ should have a peak at $\vec{q} = \pi(1, 1/\sqrt{3})$. We can also see this directly from the form of the classical spin configuration in Eq. (26). Since the two-spin correlation between sites $\vec{0} = (0,0)$ and $\vec{n}$ is equal to $\vec{S}_{\vec{0}}\cdot\vec{S}_{\vec{n}} = S^2(-1)^{m_1}$, we see from Eqs. (22) and (24) that the Fourier transform,

$$
S(\vec{q}) = \sum_{\vec{n}} e^{-i\vec{q}\cdot\vec{n}}\vec{S}_{\vec{0}}\cdot\vec{S}_{\vec{n}}, \tag{33}
$$

will have a peak at $\vec{q} = \pi(1, 1/\sqrt{3})$. We will see later that this agrees with our numerical results based on ED.

Expanding around $\vec{k} = (0,0)$, we find that

$$
\begin{aligned}
E_{\vec{k}}^2 &= S^2 a^2(J_\alpha + J_\gamma)(k_x \quad k_y)M_{\vec{k}}\begin{pmatrix} k_x \\ k_y \end{pmatrix}, \\
M &= \begin{pmatrix} J_\alpha + \frac{1}{4}(J_\gamma - J_\beta) & \frac{\sqrt{3}}{4}(J_\beta + J_\gamma) \\ \frac{\sqrt{3}}{4}(J_\beta + J_\gamma) & \frac{3}{4}(J_\gamma - J_\beta) \end{pmatrix}.
\end{aligned} \tag{34}
$$

The above analysis clearly breaks down if any of the eigenvalues of $M_{\vec{k}}$ becomes negative since that would make the energy $E_{\vec{k}}$ imaginary. This happens if

$$
\det(M_{\vec{k}}) = \frac{3}{4}(J_\alpha J_\gamma - J_\beta J_\gamma - J_\alpha J_\beta) \tag{35}
$$

turns negative. We thus conclude that the spin-wave spectrum near the ground state spin configuration given in Eq. (25) is real if

$$
\frac{1}{J_\beta} > \frac{1}{J_\alpha} + \frac{1}{J_\gamma}, \tag{36}
$$

and a transition must occur to some other phase when

$$
\frac{1}{J_\beta} = \frac{1}{J_\alpha} + \frac{1}{J_\gamma}. \tag{37}
$$

As we approach the line in Eq. (37) from the region in Eq. (36), we find from Eq. (34) that one of the spin-wave

energies remains finite while the other approaches zero as some finite constant times $\sqrt{\lambda}|\vec{k}|$, where

$$
\lambda \equiv \frac{1}{J_\beta} - \frac{1}{J_\alpha} + \frac{1}{J_\gamma}. \tag{38}
$$

The above analysis was based on an expansion of the spin Hamiltonian in Eq. (23) up to order S, assuming that the ground state expectation value of $a_{\vec{n}}^\dagger a_{\vec{n}}$ appearing in Eqs. (28) and (29) are much smaller than S. We can now check for the self-consistency of this assumption [98]. We find that

$$
\langle a_{\vec{n}}^\dagger a_{\vec{n}} \rangle \sim \int \frac{d^2 k}{E_{\vec{k}}}. \tag{39}
$$

Near the vicinity of the line in Eq. (37) and $\vec{k} = (0,0)$, we see from Eq. (38) that the integral in Eq. (39) diverges as $1/\sqrt{\lambda}$. Hence, for large S, the spin-wave analysis is expected to break down in a region appearing *before* the phase transition line where the integral in Eq. (39) is not much smaller than S. We may expect this region to form a disordered phase. We will see in the next section that the ground state phase diagram for our model with $S = 1/2$ indeed has some disordered phases lying between the ordered phases.

By permuting between the three couplings J_α, J_β, and J_γ, we find that there must be two other regions similar to Eq. (36), namely,

$$
\frac{1}{J_\alpha} > \frac{1}{J_\beta} + \frac{1}{J_\gamma} \tag{40}
$$

and

$$
\frac{1}{J_\gamma} > \frac{1}{J_\alpha} + \frac{1}{J_\beta}, \tag{41}
$$

where a possible ground state spin configuration is given by

$$
\vec{S}_{\vec{n}} = S(0, 0, (-1)^{m_2}) \tag{42}
$$

and

$$
\vec{S}_{\vec{n}} = S(0, 0, (-1)^{m_1 + m_2}), \tag{43}
$$

respectively. The three collinear ordered phases given by Eqs. (36), (40), and (41) are shown in Fig. 4 (see also Ref. [89]).

We will now briefly discuss the remaining region in Fig. 4, still setting $C = 0$. We will assume that the ground state spin configuration in this region is given by a coplanar configuration of the form

$$
\begin{aligned}
\vec{S}_{\vec{n}} &= S(\cos\phi_{\vec{n}}, \sin\phi_{\vec{n}}, 0), \\
\text{where} \quad \phi_{\vec{n}} &= m_1\phi_1 + m_2\phi_2, \tag{44}
\end{aligned}
$$

for $\vec{n} = m_1\vec{u} + m_2\vec{v}$. This implies that

$$
\begin{aligned}
\vec{S}_{\vec{n}}\cdot\vec{S}_{\vec{n}+\vec{u}} &= S^2\cos\phi_1, \\
\vec{S}_{\vec{n}}\cdot\vec{S}_{\vec{n}+\vec{v}} &= S^2\cos\phi_2, \\
\vec{S}_{\vec{n}}\cdot\vec{S}_{\vec{n}+\vec{w}} &= S^2\cos(\phi_1 + \phi_2). \tag{45}
\end{aligned}
$$

The classical ground state energy for a system with N sites is then given by

$$
E_{cl} = NS^2[J_\alpha\cos\phi_1 + J_\beta\cos\phi_2 + J_\gamma\cos(\phi_1 + \phi_2)]. \tag{46}
$$
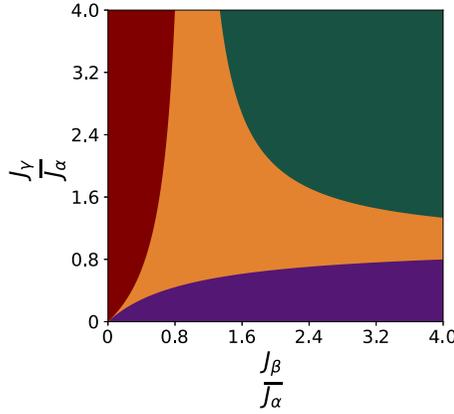
FIG. 4. The classical ground state phase diagram as a function of J_β/J_α and J_γ/J_α for $C = 0$. There are three collinear (or striped) phases where Eqs. (36) (shown in maroon), (40) (dark green), and (41) (violet) are satisfied. The rest of the diagram, shown in yellow, describes a coplanar (or spiral) phase.

Minimizing Eq. (46) with respect to the angles ϕ_1, ϕ_2, we obtain

$$J_\alpha \sin \phi_1 + J_\gamma \sin(\phi_1 + \phi_2) = 0,$$
$$J_\beta \sin \phi_2 + J_\gamma \sin(\phi_1 + \phi_2) = 0. \qquad (47)$$

Given some values of J_α, J_β, and J_γ, we can numerically solve Eqs. (47) for ϕ_1, ϕ_2 to find a classical ground state configuration. We will not discuss here the spin-wave theory about such a ground state. For $J_\alpha = J_\beta = J_\gamma$, there are two solutions of Eqs. (47) given by $\phi_1 = \phi_2 = 2\pi/3$ and $\phi_1 = \phi_2 = 4\pi/3$. We also note that the collinear spin configurations given in Eqs. (26), (42), and (43) are, after doing a rotation which transforms the $\hat{x}$ axis into the $\hat{z}$ axis, special cases of Eq. (44) corresponding to $(\phi_1, \phi_2) = (\pi, 0)$, $(0, \pi)$, and (π, π), respectively.

For the spin configuration given in Eq. (44), we have $\vec{S}_{\vec{0}} \cdot \vec{S}_{\vec{n}} = S^2 \cos(m_1 \phi_1 + m_2 \phi_2)$. Then an argument similar to the one around Eq. (33) implies that $S(\vec{q})$ will have δ-function peaks at $\vec{q} = \pm(\phi_1, (\phi_1 + 2\phi_2)/\sqrt{3})$. Equation (47) implies that the locations of the peaks will move around as the parameters J_α, J_β, and J_γ are changed. In contrast to this, we will see later that our numerical results show peaks which are fixed at $\vec{q} = \pm(2\pi/3, 2\pi/\sqrt{3})$ for all points in the coplanar phase. This is a qualitative difference between the classical (large S) and quantum ($S = 1/2$) models.

Finally, we consider the case $C \neq 0$ and equal two-spin interactions, $J_\alpha = J_\beta = J_\gamma$. Now we find that the classical ground state configuration is neither collinear nor coplanar. We assume that the ground state spin configuration is given by

$$\vec{S}_{\vec{n}} = S(\sin \theta \cos \phi_{\vec{n}}, \sin \theta \sin \phi_{\vec{n}}, \cos \theta),$$
$$\text{where } \phi_{\vec{n}} = (m_1 + m_2)\frac{2\pi}{3}, \qquad (48)$$

for $\vec{n} = m_1 \vec{u} + m_2 \vec{v}$. This implies that

$$\vec{S}_{\vec{n}} \cdot \vec{S}_{\vec{n}+\vec{u}} = \vec{S}_{\vec{n}} \cdot \vec{S}_{\vec{n}+\vec{v}} = \vec{S}_{\vec{n}} \cdot \vec{S}_{\vec{n}+\vec{w}}$$
$$= S^2 \left(\cos^2 \theta - \tfrac{1}{2} \sin^2 \theta \right), \qquad (49)$$

$$\vec{S}_{\vec{n}} \cdot \vec{S}_{\vec{n}+\vec{u}} \times \vec{S}_{\vec{n}+\vec{w}} = \vec{S}_{\vec{n}} \cdot \vec{S}_{\vec{n}+\vec{v}} \times \vec{S}_{\vec{n}+\vec{w}}$$
$$= S^3 \frac{3\sqrt{3}}{2} \cos \theta \sin^2 \theta. \qquad (50)$$

For a system with N sites, the ground state energy is then

$$E_{cl} = NS^2 \left[3J_\alpha (\cos^2 \theta - \tfrac{1}{2} \sin^2 \theta) + 3\sqrt{3}C \cos \theta \sin^2 \theta \right], \qquad (51)$$

where we have used the fact that for each site, there is one up-pointing and one down-pointing triangle. [It is important to note here that this calculation works only because the coefficient C of the three-spin term in Eq. (23) has opposite signs for the two kinds of triangles; if the sign had been the same for all triangles, the analysis of the classical ground state spin configuration would have been significantly more complicated.] Minimizing Eq. (51) with respect to θ, we obtain

$$\cos \theta = \frac{1}{2\sqrt{3}C} \left[J_\alpha - \sqrt{J_\alpha^2 + 4C^2} \right]. \qquad (52)$$

We find that for $C = 0$, $\theta = \pi/2$ which agrees with the discussion in the previous paragraph (with $\phi_1 = \phi_2 = 2\pi/3$); we thus recover a coplanar spin configuration with the expressions in Eqs. (49) and (50) being equal to $-S^2/2$ and zero, respectively. For $C/J_\alpha \to \pm\infty$, $\theta \to \arccos(-\text{sgn}(C)/\sqrt{3})$, where $\text{sgn}(C) = +1(-1)$ for $C > 0(< 0)$. Hence Eqs. (49) and (50) are equal to zero and $-\text{sgn}(C)S^3$, respectively, i.e., in each triangle the three spins are perpendicular to each other.

V. NUMERICAL ANALYSIS OF THE MODEL

Having derived the lattice Hamiltonian for our model, we will now do an ED study to look at the ground state properties as a function of the parameters $(J_\alpha, J_\beta, J_\gamma, C)$. The triangular lattice is spanned by the primitive unit cell vectors $\vec{u}$ and $\vec{v}$ as shown in Fig. 3. We choose to perform our ED calculations on a 6×6 lattice system with total number of lattice sites, $N = 36$ with periodic boundary conditions applied in both the directions. This system size is particularly well suited for our purpose since this ensures there is no frustration in the sublattice symmetry of the triangular lattice in both the directions and the number of spin-1/2's is even. This enables us to work in the zero magnetization sector for the ground state calculations. We make use of the following symmetries in the system: (i) translation along $\hat{u}$ direction, (ii) translation along $\hat{v}$ direction, (iii) total magnetization m in the $\hat{z}$ direction in spin space, and (iv) spin inversion by the operator $Z = e^{i\pi \prod_{\vec{n}} S_{\vec{n}}^x}$ which flips $S_{\vec{n}}^z \to -S_{\vec{n}}$ at every site (with $Z = 1$ for the even sector and $Z = -1$ for the odd sector).

For the ground state, we work in the momentum sector $(q_x, q_y) = (0, 0)$, zero magnetization sector $m = 0$, and even spin inversion sector with eigenvalue of $Z = 1$. In addition, for the case when $C = 0$, we also have (v) simultaneous spatial inversion symmetry P along the $\hat{u}$ and $\hat{v}$ directions. The operator $P = P_x P_y$ acting on the state takes $x \to L_x - x$ and
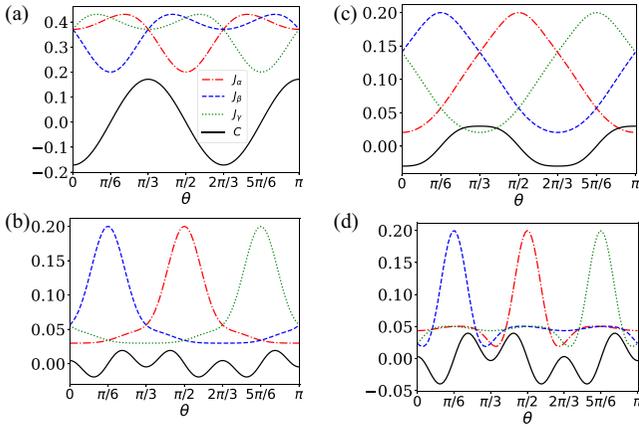
FIG. 5. Plots of $J_\alpha, J_\beta, J_\gamma$, and C as functions of θ, for $g = 1, U = 20, \omega = 17$, and $a_1 = 35$. We have taken (a) $a_2 = 30$, (b) $a_2 = 105$, (c) $a_2 = 140$, and (d) $a_2 = 175$. The values of a_2 have been chosen so as to show four qualitatively different behaviors versus θ.

FIG. 6. Plots of $J_\alpha, J_\beta, J_\gamma$, and C as functions of θ and a_2, for $g = 1, U = 20, \omega = 17$, and $a_1 = 35$. The plots show the behaviors of (a) J_α, (b) J_β, (c) J_γ, and (d) C.

$y \rightarrow L_y - y$, where L_x and L_y are the lengths of the system along $\vec{u}$ and $\vec{v}$, respectively. The ground state has an even parity for this operator enabling us to do the diagonalization in this sector. The use of these symmetries reduces the Hilbert space dimension from 2^{36} (about 6.8×10^{10}) down to about 6.3×10^7. We then examine in detail at the spatial correlation function, static spin structure function (SSSF), and fidelity susceptibility for the ground state as a function of the parameters $J_\alpha, J_\beta, J_\gamma$, and C.

For our numerical studies, we will consider an electric field which does not have time-reversal symmetry. As an example, we will take the electric field to be

$$\vec{E}(t) = \hat{n}[\mathcal{E}_1 \cos(\omega t) + \mathcal{E}_2 \sin(2\omega t)]. \qquad (53)$$

We note that this electric field is not time-reversal symmetric unless $\mathcal{E}_2 = 0$. Following the steps leading up to Eq. (2), we now find that the hopping amplitudes are given by

$$
\begin{aligned}
t_{12} &= g\, e^{(i/\omega)[a_1 \sin(\omega t) + (a_2/2)\cos(2\omega t)]\cos(\pi/3 - \theta)}, \\
t_{23} &= g\, e^{(i/\omega)[a_1 \sin(\omega t) + (a_2/2)\cos(2\omega t)]\cos(\pi - \theta)}, \\
t_{31} &= g\, e^{(i/\omega)[a_1 \sin(\omega t) + (a_2/2)\cos(2\omega t)]\cos(\pi/3 + \theta)}, \qquad (54)
\end{aligned}
$$

where $a_1 = -q\mathcal{E}_1/\hbar$ and $a_2 = q\mathcal{E}_2/\hbar$, and $t_{ji} = t_{ij}^*$.

A. Numerical values of $J_\alpha, J_\beta, J_\gamma$, and C from periodic driving

The four parameters $J_\alpha, J_\beta, J_\gamma$, and C depend on the amplitudes of driving a_1 and a_2, the frequency of driving ω, the direction of the electric field θ, and the interaction strength U. We will set $g = 1$ in all the numerical calculations. A simple parameter to vary in an experimental setup would be the electric field direction. Hence, we first fix the values of a_1, a_2, ω, and U and look at the variation of $J_\alpha, J_\beta, J_\gamma$, and C with θ. Figure 5 shows the plots of these parameters obtained using the expressions from third-order perturbation theory given in Eq. (20). We notice that the couplings J_α, J_β, and J_γ vary with a periodicity of π. Further, the values of J_α, J_β, and J_γ get cyclically interchanged when θ changes by $\pi/3$ due to the underlying triangular lattice structure. The periodicity of C on the other hand is $2\pi/3$, and its sign
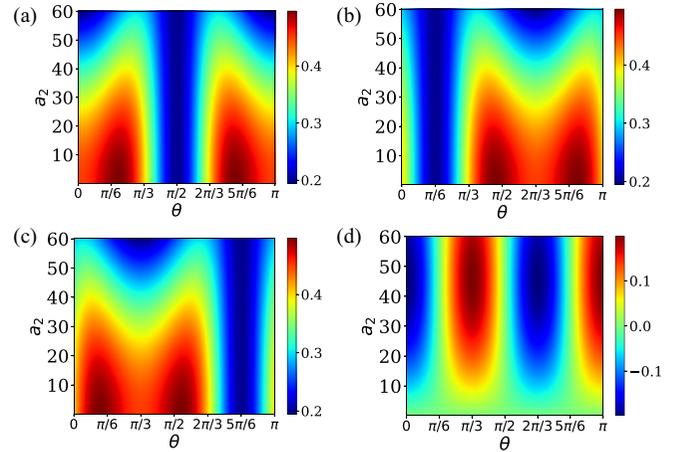
changes when θ changes by π. In Fig. 5(a) for $a_2 = 30$, we can see that there are interesting points at $\theta = \pi/3$ and $2\pi/3$ where the three two-spin coupling parameters have the same value. The value of C at these points is also the largest in magnitude, equal to about 0.15. In Fig. 5(b), we see ranges of θ where the magnitude of C is greater than one of the nearest-neighbor couplings. In Figs. 5(c) and 5(d) we notice that one of the coupling parameters is much larger than the other two. We also observe in Figs. 5(c) and 5(d) that one or two of the coupling parameters has almost the same value over a range of θ.

We note in Fig. 5 that whenever θ is equal to $(2\pi n/3) \pm \pi/6$ (where n is an integer), two of the J's are equal and $C = 0$. This is because for these values of θ, the electric field is perpendicular to one of the sides of each triangle. Then the system is invariant under a reflection about the direction of the electric field. Hence the two J's which are related by the reflection must be equal, and C must vanish since the chiral three-spin term is odd under the reflection.

The variation of the four couplings as a function of both a_2 and θ is shown in Fig. 6, where we have fixed $g = 1, U = 20, \omega = 17$, and $a_1 = 35$. We have varied a_2 from 0 to 60 and θ from 0 to π. This interval of θ is sufficient to clearly show the periodicity of $J_\alpha, J_\beta, J_\gamma$, and C. We again see from these plots that J_α, J_β, and J_γ get cyclically interchanged as θ changes by $\pi/3$, while C has a period of $2\pi/3$.

In Fig. 7, we show plots of the couplings as functions of θ obtained directly from the Floquet operator for $g = 1, U = 20, \omega = 17$, and $a_1 = 35$, and $a_2 = 30$. This calculation is done as follows. We consider a triangle of three sites containing three electrons, two with spin-up and one with spin-down; the basis states are shown in Fig. 2. We first calculate the Floquet operator U_T in Eq. (7) by discretizing the time t and multiplying N terms with time steps $\Delta t = T/N$ (we have taken $N = 201$). We then examine the nine eigenstates of U_T and find which three of them have the smallest amplitudes of the states with doubly occupied sites (the last six states in Fig. 2). We truncate these eigenstates to states with only singly occupied sites (the first three states in Fig. 2) and carry out
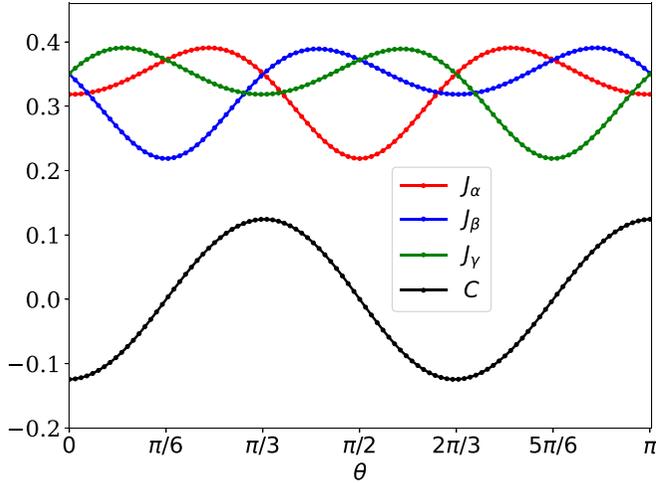
FIG. 7. Plots of J_α, J_β, J_γ, and C as functions of θ, for $g = 1$, $U = 20$, $\omega = 17$, $a_1 = 35$, and $a_2 = 30$, obtained by a numerical calculation of the Floquet operator for a single triangle with two spin-up electrons and one spin-down electron, and truncating its eigenvalues and eigenvectors to states with only singly occupied sites. The figure shows a good match with Fig. 5(a) obtained from the third-order effective Hamiltonian presented in Eq. (20).

a Gram-Schmidt orthogonalization to obtain three states $|\psi_i\rangle$, $i = 1, 2, 3$ (the orthogonalization alters the states only slightly since the amplitudes of the six states which have been left out are small). Using the states $|\psi_i\rangle$ and their corresponding Floquet quasienergies ϵ_i (these lie near zero since we have chosen g to be much smaller than U and ω), we construct the effective Hamiltonian

$$H_\triangle^{\text{eff}} = \sum_{i=1}^{3} \epsilon_i |\psi_i\rangle\langle\psi_i|. \tag{55}$$

We then fit this to the form given in Eq. (18) to extract J_α, J_β, J_γ, and C. These are plotted in Fig. 7. Note that these plots also exhibit the symmetries mentioned above for various values of θ. A comparison between Figs. 5(a) and 7 shows a good match, indicating that the results that we have obtained from the third-order effective Hamiltonian in Eq. (20) agree well with exact numerical calculations.

B. Classification of different phases using static spin structure function

The numerical values of the parameters J_α, J_β, J_γ, and C obtained for different driving parameters give us an idea of the ranges of values that they can have. To find the different phases of the system using ED, we have varied the parameters J_β, J_γ, and C independently, yet consistent with the values obtained by driving. (We have fixed $J_\alpha = 1$ for convenience.) For each set of parameters, we have calculated the static two-spin correlation function in the ground state, given by the formula $C(\vec{r}_n, \vec{r}_0) = C(\vec{r}_n - \vec{r}_0) = \langle \vec{S}_0 \cdot \vec{S}_n \rangle$. This correlation function tells us the kind of order present in the ground state. In the case of ordered ground states, the SSSF, defined as the

Fourier transform of the correlation function

$$S(\vec{q}) = \frac{1}{\sqrt{N}} \sum_{\vec{r}_n} e^{-i\vec{q}\cdot(\vec{r}_n - \vec{r}_0)} C(\vec{r}_n - \vec{r}_0) \tag{56}$$

(where N is the number of lattice sites) peaks sharply at particular points $\vec{q}$ in the Brillouin zone. The positions of these peaks indicates the nature of the order. On the other hand, SSSF does not have a well-defined peak at any point in the Brillouin zone for a disordered ground state.

For our choice of the lattice vectors $\vec{u}$ and $\vec{v}$, the Brillouin zone in reciprocal space in spanned by the reciprocal lattice vectors $\vec{q}_x$ and $\vec{q}_y$ which run from 0 to 2π and 0 to $4\pi/\sqrt{3}$, respectively, as shown in Fig. 8. From the SSSF calculations we have classified a total of seven possible phases, of which four are ordered and the other three are disordered. We have shown representative plots of SSSF for each of these phases in Fig. 8. To summarize the ordered phases, we have shown the $\vec{q}$ points where the SSSF has peaks for the different ordered phases in the top left figure in Fig. 8. In Sec. V D, we will confirm the different phases obtained from the SSSF using other quantities like the fidelity susceptibility and real-space correlation values at large distances.

C. Ground state phase diagram

We now present the phase diagram as a function of J_β/J_α and J_γ/J_α in Fig. 9. We saw in Sec. V A that the values obtained for C by driving is usually small compared to $(J_\alpha, J_\beta,$ and $J_\gamma)$, except in some small regions where the C is comparable to one of the couplings. Further, we have found numerically that the SSSF calculated for the ground state does not change significantly on including the values of C obtained by driving even when it is comparable to one of the two-spin couplings. Hence the phase diagram is practically independent of the value of C. We have therefore set $C = 0$ in Fig. 9.

D. Verification of different phases: Fidelity susceptibility, minimum real-space correlation function, and energy levels

Quantum phase transitions can often be captured by looking at the ground-state fidelity as a function of the parameters of the system. Fidelity is a concept borrowed from quantum information theory. It is defined as

$$\mathcal{F}(\lambda) = |\langle\psi_0(\lambda)|\psi_0(\lambda + \delta\lambda)\rangle|, \tag{57}$$

where $|\psi_0(\lambda)\rangle$ and $|\psi_0(\lambda + \delta\lambda)\rangle$ are the ground states of the many-body Hamiltonian H with slightly different parameters λ and $\lambda + \delta\lambda$, respectively. For a fixed and small value of $\delta\lambda$, $\mathcal{F}$ generally exhibits a prominent dip whenever a phase transition occurs between λ and $\lambda + \delta\lambda$. As a result, the second derivative of the fidelity with respect to λ usually shows large changes near a quantum critical point. This leads us to define another measure called the fidelity susceptibility [101,102]

$$\chi_F(\lambda) = -\frac{\partial^2 \ln \mathcal{F}}{\partial(\delta\lambda)^2}\bigg|_{\delta\lambda \to 0}. \tag{58}$$

At a critical point χ_F generally shows a maximum or a divergence. To confirm the phase boundaries shown in Fig. 9, we have chosen three vertical lines A, B, and C which, taken together, cover all the seven phases, and we have calculated
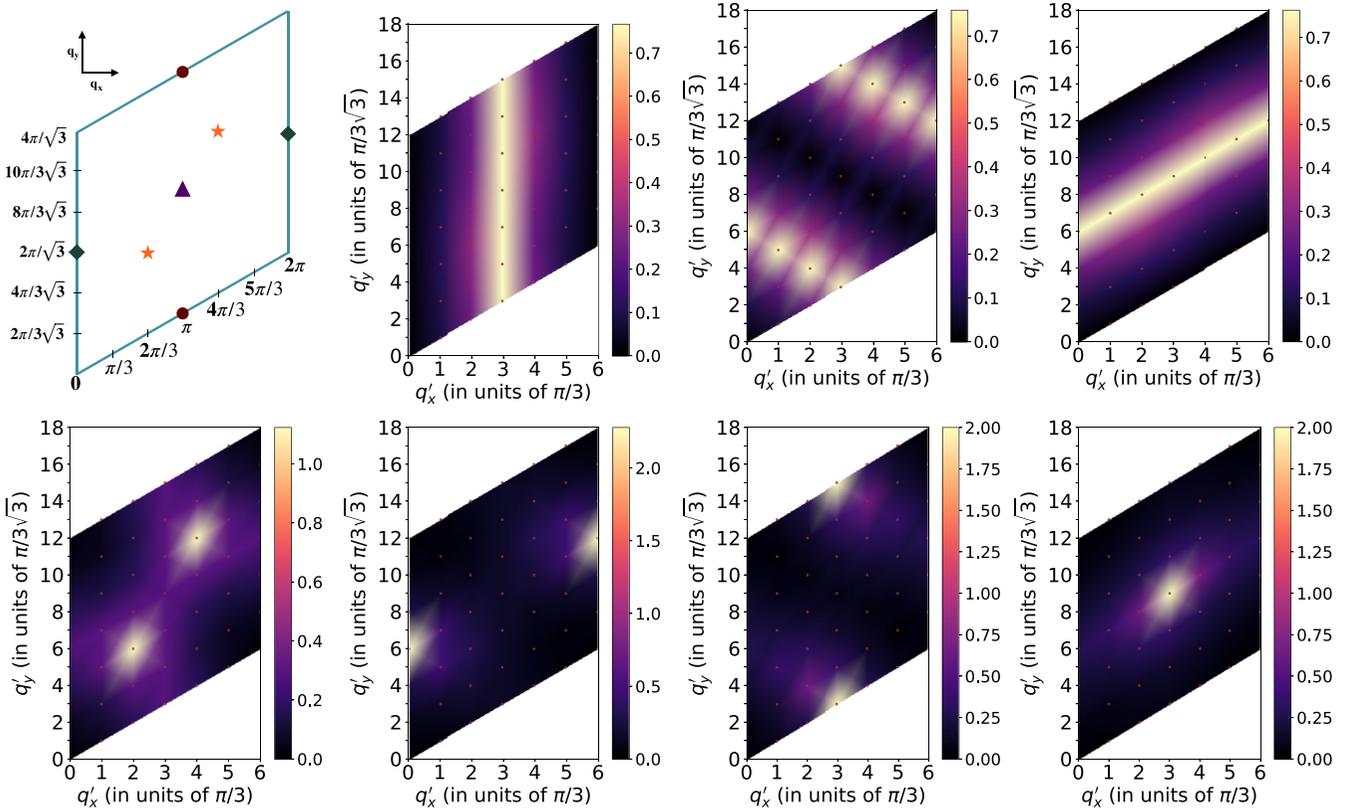
FIG. 8. The first figure in the top row shows the locations of the peaks in the SSSF for different ordered phases in the Brillouin zone of the triangular lattice. The peaks at $(\pi/3, 2\pi/\sqrt{3})$ and $(4\pi/3, 4\pi/\sqrt{3})$ indicated by ★ correspond to the peaks in SSSF in the spiral phase, as shown in the first figure in the bottom row. The peaks located at the points marked at $(0, 2\pi/\sqrt{3})$ and $(2\pi, 4\pi/\sqrt{3})$ shown by ◆, $(\pi, \pi/\sqrt{3})$ and $(\pi, 5\pi/\sqrt{3})$ shown by ●, and $(\pi, 3\pi/\sqrt{3})$ represented by ▲ correspond to the collinear phases called stripe $\vec{u}$, stripe $\vec{v}$, and stripe $\vec{w}$, and the last three figures in the bottom row show plots of the SSSF in these three phases, respectively. The SSSFs for the spin-liquid phases are shown in the last three figures in the top row. We see that the largest values of the SSSF are spread out over many $\vec{q}$ points in the spin-liquid phases. In the third figure in the top row, the apparent fringes are only due to the interpolation scheme used while plotting, and the SSSF values are actually highest all along the two parallel lines in this figure.

χ_F along these lines. The top row in Fig. 10 shows plots of χ_F as a function of the parameter J_γ. The locations of phase boundaries obtained from the peaks in χ_F and from the SSSF calculations agree well with each other. For line A, with $J_\beta = 0.6$, we see from Fig. 9 that it passes from stripe $\vec{w}$ through a spin liquid to stripe $\vec{v}$. The fidelity susceptibility along this line shows two maxima at $J_\gamma = 0.475$ and 0.77 which mark the phase transitions to and from the spin-liquid phase. Similarly line C shows maxima in χ_F at $J_\gamma = 0.775$ and 1.5 indicating a similar phase transition from stripe $\vec{w}$ through a spin liquid to stripe $\vec{u}$. On line B, however, we find a divergence in χ_F at $J_\gamma = 0.82$ and 1.18. These points match the phase transitions seen in Fig. 9 when the system goes from stripe $\vec{w}$ to the spiral phase to a spin liquid. The divergences in χ_F in this case suggests discontinuous transitions and these may occur because the transitions here are from a spiral phase (which has a very different kind of structure as shown by the SSSF in Fig. 8) to a striped phase or to a spin liquid.

We have also used the minimum value of the two-spin correlation function (the value at the largest possible distance between two spins, namely, halfway across the system) as a tool to distinguish between different phases. In the ordered phases, $\langle \vec{S}_{\vec{0}} \cdot \vec{S}_{\vec{n}} \rangle$ at large separation $|\vec{n}|$ goes to a finite value,

while in a spin-liquid phase the correlation approaches zero quickly with increasing separation. The minimum value of the two-spin correlation function captures the correlation at the largest distance possible in our 6×6 lattice. In the bottom row of Fig. 10 we have shown the variation of the minimum correlation versus J_γ along the lines A, B, and C. In each of the lines we see a rapid drop in the value whenever it is in a spin-liquid phase. The minimum correlation is of the order of 10^{-1}–10^{-2} in the ordered phases and of the order of 10^{-3}–10^{-4} in the spin-liquid phases. The phase boundaries obtained by this method are not as sharp as ones obtained from χ_F; however, they still agree quite well with each other. Both the fidelity susceptibility and the minimum value of the real-space correlation function in Fig. 10 suggest that transitions between a striped phase and a spin liquid are continuous (lines A and C), while a transition between the spiral phase and either a striped phase or a spin liquid is discontinuous (line B).

We have also studied the first excited state energy along the lines A, B, and C as shown in Fig. 11. While the ground state has momentum $(0,0)$ and is in the even parity ($P = 1$) and even spin-inversion sector ($Z = 1$) for all values of the parameters, the excited state has different momenta and lies
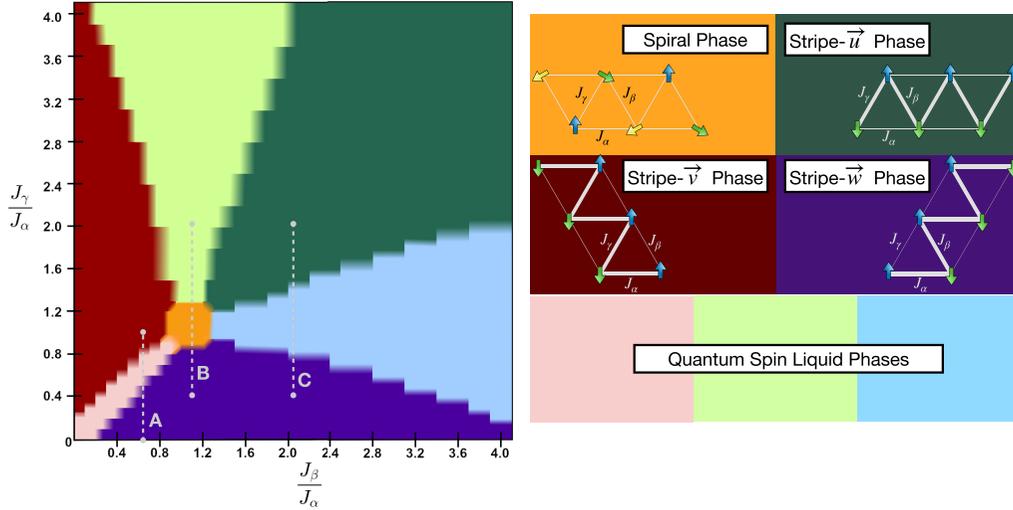
FIG. 9. The phase diagram of the effective spin model as a function of J_β/J_α and J_γ/J_α, for $C = 0$. The different phases classified by the SSSF are shown in the figure on the right. We have seven phases altogether, of which four are ordered and three are disordered or spin-liquid phases. The stripe phases are separated from each other by intermediate spin-liquid phases as shown in the figure on the left. The phases boundaries remain the same on interchanging J_β and J_γ, only the directions of the spin configurations change as expected from the geometry of the triangular lattice. We have marked three lines A, B, and C in the phase diagram which encompass all seven phases. We have calculated the fidelity susceptibility, real-space correlation function, and energy gaps along these lines to verify the phase boundaries obtained using SSSF. Note that we used a resolution of 0.1 in both directions while constructing the phase diagram; this explains the discrete stair-like structure of the phase boundaries.

in different parity sectors in different regions in the parameter space. Along line A, which is at $J_\beta = 0.6$, we find that as we vary J_γ from 0 to 1, the excited state is in the momentum sector $\vec{q} = \vec{q}_3 = (\pi, 3\pi/\sqrt{3})$ with $P = 1$ and $Z = -1$. We then have a transition at $J_\gamma = J_\beta = 0.6$ after which the excited state has momentum $\vec{q} = \vec{q}_2 = (\pi, \pi/\sqrt{3})$ with $P = -1$ and $Z = -1$. The plot for line C is quite similar. Here we have fixed

$J_\beta = 2.0$ and J_γ is varied from 0.4 to 2. The symmetry sector of the excited state changes from $\vec{q} = \vec{q}_3 = (\pi, 3\pi/\sqrt{3})$, $P = 1$, $Z = -1$ to $\vec{q} = \vec{q}_1 = (0, 2\pi/\sqrt{3})$, $P = -1$, $Z = -1$ at $J_\gamma = 1$. Along both lines A and C, we cannot comment on the nature of the transition from ordered to spin liquid or vice versa by looking at the energy gap between the ground state and first excited state. However, we expect that in the
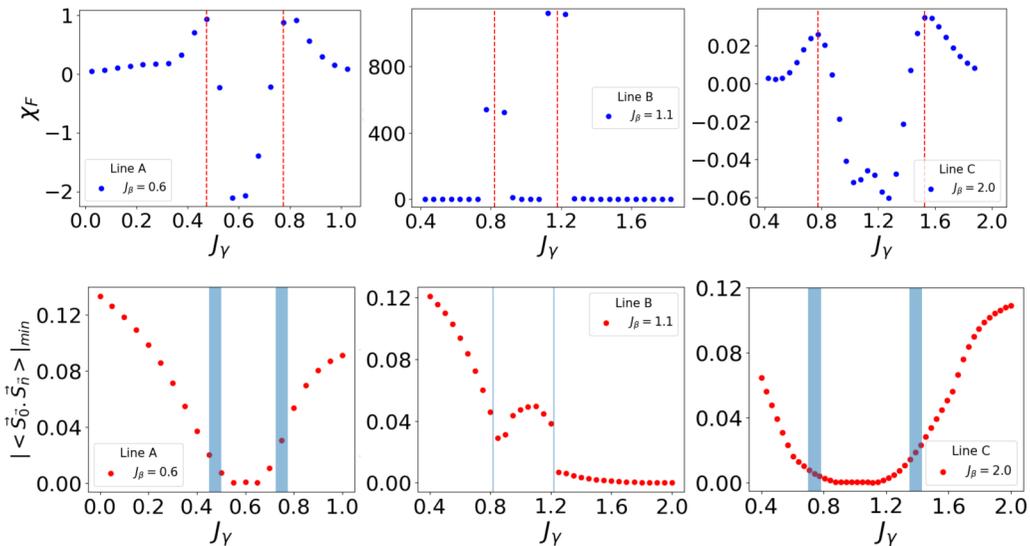
FIG. 10. Plots of the fidelity susceptibility (top row) and the minimum value of the real-space correlation function (bottom row) along the lines A, B, and C shown in Fig. 9. The fidelity susceptibility shows significant changes at all the phase transition lines. However, the change is extremely large at the transitions on line B; note that the scale of the y axis in the plot for line B is quite different from the scales for lines A and C. Similarly, the minimum value of the real-space correlation function seems to change continuously at the transitions on lines A and C but discontinuously at the transitions on line B.
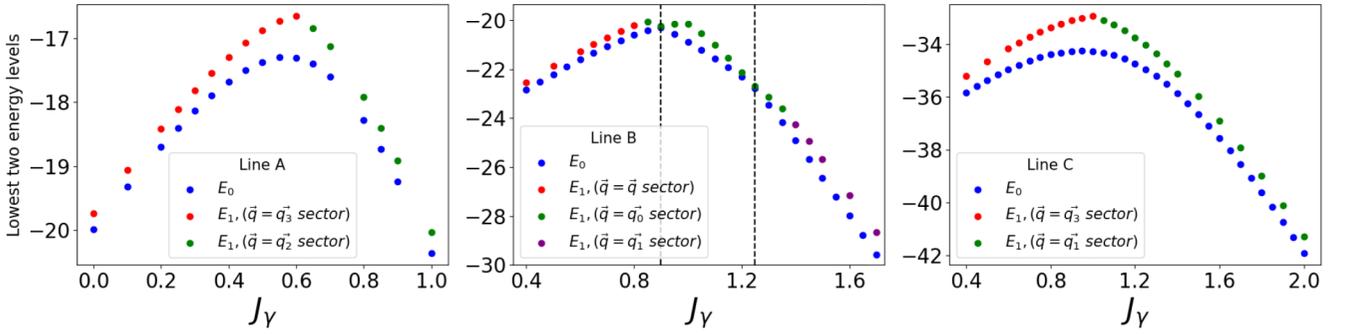
FIG. 11. Plots of the ground state and first excited state energies along the lines A, B, and C shown in Fig. 9. The gap between the ground state and first excited state remains finite all along lines A and C but becomes close to zero at the transitions on line B. The ground state always lies in the symmetry sector with even parity ($P = 1$), even spin inversion ($Z = 1$) and momentum $(0,0)$. However, the symmetry sectors of the excited state changes as J_γ is varied. For line A, the excited state has $P = -1$ and $Z = -1$ with the momentum sector changing from $\vec{q}_3 = (\pi, 3\pi/\sqrt{3})$ to $\vec{q}_2 = (\pi, \pi/\sqrt{3})$ at $J_\gamma = 0.6$. Similarly for line C at $J_\gamma = 1.0$, the momentum sector switches from $\vec{q}_3$ to $\vec{q}_1 = (0, 2\pi/\sqrt{3})$ with $P = -1$ and $Z = -1$. Along line B, the excited state changes once from $\vec{q} = \vec{q}_3$, $P = 1$, $Z = -1$ to $\vec{q} = \vec{q}_0 = (0, 0)$, $P = 1$, $Z = 1$, and then again to $\vec{q} = \vec{q}_1$, $P = -1$, $Z = -1$. These changes occur in the vicinity of the energy gap closing points.

stripe phases the energy gap will vanish in the thermodynamic limit since spin-wave theory about the classical stripe phases predicts a gapless dispersion. For line B, we have fixed $J_\beta = 1.1$ and varied J_γ from 0.4 to 2. This line contains the spiral phase and the energy gap closes at its phase boundaries. Along this line the excited state changes its symmetry sector twice, once from $\vec{q} = \vec{q}_3$, $P = 1$, $Z = -1$ to $\vec{q} = \vec{q}_0 = (0, 0)$, $P = 1$, $Z = 1$, and then again to $\vec{q} = \vec{q}_1$, $P = -1$, $Z = -1$. These changes occur near the transition from stripe-w phase to the spiral phase and from the spiral phase to one of the spin-liquid phases, respectively. For this line also we expect that the energy gap will vanish in the thermodynamic limit for the ordered phases. Moreover, the spin-liquid phase on line B has a small gap (of the order of or smaller than the inverse system size); hence it is like to be gapless in the thermodynamic limit. For line B, we have shown in Fig. 12 how $S(\vec{q})$ varies for the $\vec{q}$ points in the three phases that the line covers. We see that the maximum value of $S_{\vec{q}}$ is at $\vec{q} = (\pi, 3\pi/\sqrt{3})$ corresponding

to the stripe-$\vec{w}$ phase until $J_\gamma = 0.82$, and at $(2\pi/3, 2\pi/\sqrt{3})$ and $(4\pi/3, 4\pi/\sqrt{3})$ corresponding to the spiral phase until $J_\gamma = 1.2$. Beyond this we find that the maximum value of $S_{\vec{q}}$ is spread across the two lines as shown in the inset of Fig. 12 which correspond to a spin-liquid phase. This further confirms the phase boundaries for this line.

We note that all the three spin-liquid phases are similar in the sense that one can obtain one from the other by permuting or exchanging the parameters J_α, J_β, and J_γ. Hence, since the spin-liquid phase on line B appears to be gapless (Fig. 11), all the spin-liquid phases are likely to be gapless.

E. Effect of C

Although the chiral three-spin term with coefficient C does not seem to play an important role in the phase transitions between ordered and spin-liquid phases, it does have some effect on the ground state. The classical calculation in the large-S limit suggests that the effect of the three-spin term is to make the spin configuration noncoplanar in every triangle. In addition, the staggered structure of the three-spin term for up- and down-pointing triangles ensures that the energy can be minimized for all triangles simultaneously by having a particular noncoplanar three-sublattice order. We can measure this noncoplanarity using an order parameter given by the ground state expectation value of the chiral three-spin term $\vec{S}_1 \cdot \vec{S}_2 \times \vec{S}_3$ on any triangle in the lattice, taken in an anti-clockwise (clockwise) sense for up-pointing (down-pointing) triangles. This is shown in Fig. 13 for values of C (and the corresponding values of J_α, J_β and J_γ) obtained as a function of θ in Fig. 5(a). As expected, we find that this order parameter is an odd function of C and it vanishes if $C = 0$.

VI. DISCUSSION

In this paper we have studied the effects of a periodically varying in-plane electric field on the Hubbard model at half filling on a triangular lattice. In the limit that the nearest-neighbor hopping amplitude g is much smaller than the interaction strength U and the driving frequency ω, we

FIG. 12. SSSF plotted at different values of $\vec{q}$ in the Brillouin zone which are shown in the inset. The SSSF is plotted along line B in Fig. 9, with $J_\alpha = 1$ and $J_\beta = 1.1$ held fixed. Line B goes across three phases as J_γ is increased, and the SSSF shows corresponding transitions in its values at the two phase boundaries. $S(\vec{q})$ has the maximum value for the stripe-$\vec{v}$ phase at $\vec{q} =$ ▲ from $J_\gamma = 0$ to $J_\gamma \simeq 0.82$, for the spiral phase at $\vec{q} =$ ★ from $J_\gamma \simeq 0.82$ to $J_\gamma \simeq 1.2$, and for the spin-liquid phase at $\vec{q} =$ ☐ from $J_\gamma \simeq 1.2$ onwards.

FIG. 13. Plot of chiral three-spin term $\langle \vec{S}_1 \cdot \vec{S}_2 \times \vec{S}_3 \rangle$ for any triangle versus C, for a system with $g = 1$, $U = 20$, $\omega = 17$, $a_1 = 35$, and $a_2 = 30$.

have used a Floquet perturbation theory to derive the effective Hamiltonian up to order g^3 in the spin sector, namely, the sector of states in which all sites are singly occupied. Assuming that there is no resonance, i.e., U is not close to an integer multiple of ω, we find that the Hamiltonian is given by a sum of nearest-neighbor Heisenberg interactions at orders g^2 and g^3, and, if the electric field is not time-reversal symmetric, a chiral three-spin interaction on each triangle at order g^3. Indeed, the reason we chose to study the Hubbard model on a triangular lattice is that it is known that a magnetic field which is perpendicular to the plane of the lattice gives rise, at order g^3 in time-independent perturbation theory, to a chiral three-spin interaction with a coefficient which depends on the magnetic flux passing through each triangle [97]. Thus an oscillating electric field in our model can simulate the effect of a magnetic flux in a time-independent system. Interestingly however, while the sign of the three-spin term written in the anticlockwise direction is the same for up- and down-pointing triangles in the time-independent magnetic flux problem, the sign is opposite in the two kinds of triangles in our periodically driven problem.

In our numerical calculations we have chosen the oscillating electric field to be linearly polarized with two different frequencies in order to break time-reversal symmetry. This is in contrast to earlier work which showed that chiral three-spin terms can be generated when circularly polarized radiation with a single frequency is applied to certain frustrated Mott insulators, and these terms appear at fourth order in g [94–96,103]. It has also been shown that partially polarized and unpolarized radiation with a single frequency can generate chiral three-spin and other multi-spin terms at fourth order in g in various Mott insulators [104,105].

The coefficients of the two-spin Heisenberg interactions in our effective spin Hamiltonian are found to have different values, J_α, J_β, J_γ, for bonds pointing along the three different directions on the triangular lattice. The values of J_α, J_β, J_γ and the coefficient C of the three-spin term depend on all the driving parameters such as the amplitude and frequency of driving and the direction of the electric field. (Typically, C is found to be smaller than J_α, J_β and J_γ.) We thus obtain an interesting spin model whose parameters can all be tuned by

the driving. We then study this spin model in detail. We first carry out a classical analysis (by taking the spin at site to be very large instead of $1/2$) to find the possible ground state spin configurations. Depending on the spin model parameters we find that there are three collinear and one coplanar ordered state. We then use spin-wave theory to find the excitation spectrum about one of the collinear ground states; we find that this theory breaks down close to the transition to a different phase, which hints at the possibility of some disordered phases.

Next, we use ED to numerically study systems with 36 sites with periodic boundary conditions. We concentrate on the ground state and use various symmetries of the system to reduce the Hilbert space dimension, by working in the sector with zero momentum in both directions, zero total spin in the z direction, even spin inversion, and, if $C = 0$, even spatial inversion. After finding the ground state, we look at the two-spin correlation function in real space, the SSSF, and the fidelity susceptibility. We also look at the energies of the ground state and the lowest excited state. Putting together all this information, we find a rich ground state phase diagram consisting of three collinear and one coplanar ordered phase (in agreement with the classical analysis) as well as three disordered phases. We find transitions between the coplanar phase and all the other six phases. In each of the ordered phases, the SSSF in momentum space has a peak at one or two points in the Brillouin zone, while in each of the disordered phases, the SSSF is large along some lines. Away from the phase transition lines, the peak values of the SSSF are significantly smaller in the disordered phases compared to the ordered phases. In real space, the two-spin correlation function at the largest possible separation (namely, between two points separated by half the system size in both directions) is found to be finite in the ordered phases and very small in the disordered phase; this is expected for systems with and without long-range order respectively. The ground state fidelity susceptibility is found shows significant changes whenever a phase transition line is crossed; the changes are much larger at the transitions between the coplanar phase and the other phases, compared to the changes which occur at transitions between collinear ordered and disordered phases. This is related to the observation that the ground state and first excited state remain well separated in energy for at transitions between collinear ordered and disordered phases but come very close to each other at transitions between the coplanar phase and the other phases. For $C = 0$, our phase diagram is in broad agreement with the ones reported in Refs. [87–89]. Finally, we have found that the values of C that are typically generated by periodic driving are not large enough to significantly modify the ground state phase diagram.

The effective Hamiltonian that we have studied in this paper applies only to the spin sector where each site is occupied by a single electron. This description is valid in a prethermal regime, and it is known that in systems with short-range interactions, the duration of this regime is exponentially large when the frequency is much larger than the hopping [106–108], as we have assumed in our numerical calculations. Eventually, after an exponentially long time, the periodic driving is expected to heat up our system to infinite temperature where all states are equally probable; then the analysis in this paper will break down.

In summary, our work proposes a way of simulating a tunable spin model by periodically driving a fermionic system with strong interactions. Earlier theoretical works have studied the effects of chiral three-spin terms generated by circularly polarized radiation applied to kagome Mott insulators such as herbertsmithite [94,95] and magnetic systems like CrI_3 [96]. The values of the Hubbard interaction U and the photon energy $\hbar\omega$ considered in these systems are typically of the order of 1 eV, and the ratio U/g is about 20–30.

In this work we have considered a closed system which is not coupled to a thermal bath at some temperature. Coupling to a bath is generally expected to lead to a Floquet-Gibbs distribution of the states when a periodically driven system is not integrable [109,110]. The effects of a bath on our system may be an interesting problem for future studies.

We would like to end by mentioning some of the recent experiments where spin-liquid and magnetically ordered phases have been realized on a triangular lattice. When ultracold bosonic atoms on a triangular optical lattice are periodically shaken in an elliptical manner [111,112], it is found that the system is effectively governed by a spin model whose couplings can be tuned at will. This allows for the realization of various ordered and disordered phases at high enough temperatures. On the other hand, there are several magnetic materials like the organic salts $Me_{4-n}Et_nPn[Pd(dmit)_2]_2$, [113] TMTTF, [114] and $BaAg_2Cu[VO_4]_2$ [115] where first-principle calculations have shown that they can be described by a triangular lattice antiferromagnet with spatially anisotropic exchange couplings similar to the ones studied in our paper.

[1] D. H. Dunlap and V. M. Kenkre, Phys. Rev. B **34**, 3625 (1986).

[2] F. Grossmann, T. Dittrich, P. Jung, and P. Hänggi, Phys. Rev. Lett. **67**, 516 (1991).

[3] Y. Kayanuma, Phys. Rev. A **50**, 843 (1994).

[4] A. Das, Phys. Rev. B **82**, 172402 (2010); S. Bhattacharyya, A. Das, and S. Dasgupta, *ibid.* **86**, 054410 (2012).

[5] A. Russomanno, A. Silva, and G. E. Santoro, Phys. Rev. Lett. **109**, 257201 (2012).

[6] A. Lazarides, A. Das, and R. Moessner, Phys. Rev. Lett. **112**, 150401 (2014).

[7] T. Nag, S. Roy, A. Dutta, and D. Sen, Phys. Rev. B **89**, 165425 (2014); T. Nag, D. Sen, and A. Dutta, Phys. Rev. A **91**, 063607 (2015).

[8] S. Sharma, A. Russomanno, G. E. Santoro, and A. Dutta, Europhys. Lett. **106** (2014) 67003; A. Russomanno, S. Sharma, A. Dutta, and G. E. Santoro, J. Stat. Mech. (2015) P08030.

[9] A. Dutta, G. Aeppli, B. K. Chakrabarti, U. Divakaran, T. Rosenbaum, and D. Sen, *Quantum Phase Transitions in Transverse Field Spin Models: From Statistical Physics to Quantum Information* (Cambridge University Press, Cambridge, 2015).

[10] S. Mondal, D. Pekker, and K. Sengupta, Europhys. Lett. **100**, 60007 (2012); U. Divakaran and K. Sengupta, Phys. Rev. B **90**, 184303 (2014); S. Kar, B. Mukherjee, and K. Sengupta, *ibid.* **94**, 075130 (2016).

[11] A. Agarwala, U. Bhattacharya, A. Dutta, and D. Sen, Phys. Rev. B **93**, 174301 (2016).

[12] A. Agarwala and D. Sen, Phys. Rev. B **95**, 014305 (2017).

[13] B. Mukherjee, P. Mohan, D. Sen, and K. Sengupta, Phys. Rev. B **97**, 205415 (2018).

[14] A. Lubatsch and R. Frank, Symmetry **11**, 1246 (2019); Eur. Phys. J. B **92**, 215 (2019).

[15] A. Udupa, K. Sengupta, and D. Sen, Phys. Rev. B **102**, 045419 (2020).

[16] S. Lubini, L. Chirondojan, G. L. Oppo, A. Politi, and P. Politi, Phys. Rev. Lett. **122**, 084102 (2019).

[17] B. Mukherjee, S. Nandy, A. Sen, D. Sen, and K. Sengupta, Phys. Rev. B **101**, 245107 (2020).

[18] A. Haldar, D. Sen, R. Moessner, and A. Das, Phys. Rev. X **11**, 021008 (2021).

[19] A. Eckardt, C. Weiss, and M. Holthaus, Phys. Rev. Lett. **95**, 260404 (2005).

[20] A. Rapp, X. Deng, and L. Santos, Phys. Rev. Lett. **109**, 203005 (2012).

[21] W. Zheng, B. Liu, J. Miao, C. Chin, and H. Zhai, Phys. Rev. Lett. **113**, 155303 (2014).

[22] S. Greschner, L. Santos, and D. Poletti, Phys. Rev. Lett. **113**, 183002 (2014).

[23] A. Lazarides, A. Das, and R. Moessner, Phys. Rev. E **90**, 012110 (2014).

[24] L. D'Alessio and M. Rigol, Phys. Rev. X **4**, 041048 (2014).

[25] P. Ponte, Z. Papić, F. Huveneers, and D. A. Abanin, Phys. Rev. Lett. **114**, 140401 (2015).

[26] A. Lazarides, A. Das, and R. Moessner, Phys. Rev. Lett. **115**, 030402 (2015).

[27] P. Ponte, A. Chandran, Z. Papić, and D. A. Abanin, Ann. Phys. **353**, 196 (2015).

[28] A. Eckardt and E. Anisimovas, New J. Phys. **17**, 093039 (2015).

[29] M. Bukov, M. Kolodrubetz, and A. Polkovnikov, Phys. Rev. Lett. **116**, 125301 (2016).

[30] V. Khemani, A. Lazarides, R. Moessner, and S. L. Sondhi, Phys. Rev. Lett. **116**, 250401 (2016).

[31] C. W. von Keyserlingk, V. Khemani, and S. L. Sondhi, Phys. Rev. B **94**, 085112 (2016).

[32] D. V. Else, B. Bauer, and C. Nayak, Phys. Rev. Lett. **117**, 090402 (2016); Phys. Rev. X **7**, 011026 (2017).

[33] A. P. Itin and M. I. Katsnelson, Phys. Rev. Lett. **115**, 075301 (2015).

[34] T. Mikami, S. Kitamura, K. Yasuda, N. Tsuji, T. Oka, and H. Aoki, Phys. Rev. B **93**, 144307 (2016).

[35] W. Su, M. N. Chen, L. B. Shao, L. Sheng, and D. Y. Xing, Phys. Rev. B **94**, 075145 (2016).

[36] M. Raciunas, G. Zlabys, A. Eckardt, and E. Anisimovas, Phys. Rev. A **93**, 043618 (2016).

[37] J. H. Mentink, J. Phys.: Condens. Matter **29**, 453001 (2017).

[38] R. Ghosh, B. Mukherjee, and K. Sengupta, Phys. Rev. B **102**, 235114 (2020).

[39] I. Bloch, Nat. Phys. **1**, 23 (2005).

[40] T. Kitagawa, M. A. Broome, A. Fedrizzi, M. S. Rudner, E. Berg, I. Kassal, A. Aspuru-Guzik, E. Demler, and A. G. White, Nat. Commun. **3**, 882 (2012).

[41] L. Tarruell, D. Greif, T. Uehlinger, G. Jotzu, and T. Esslinger, Nature (London) **483**, 302 (2012).

[42] M. C. Rechtsman, J. M. Zeuner, Y. Plotnik, Y. Lumer, D. Podolsky, S. Nolte, F. Dreisow, M. Segev, and A. Szameit, Nature (London) **496**, 196 (2013); M. C. Rechtsman, Y. Plotnik, J. M. Zeuner, D. Song, Z. Chen, A. Szameit, and M. Segev, Phys. Rev. Lett. **111**, 103901 (2013); Y. Plotnik, M. C. Rechtsman, D. Song, M. Heinrich, J. M. Zeuner, S. Nolte, Y. Lumer, N. Malkova, J. Xu, A. Szameit, Z. Chen, and M. Segev, Nat. Mater. **13**, 57 (2014).

[43] S. S. Hedge, H. Katiyar, T. S. Mahesh, and A. Das, Phys. Rev. B **90**, 174407 (2014).

[44] T. Langen, R. Geiger, and J. Schmiedmayer, Annu. Rev. Condens. Matter Phys. **6**, 201 (2015).

[45] G. Jotzu, M. Messer, R. Desbuquois, M. Lebrat, T. Uehlinger, D. Greif, and T. Esslinger, Nature (London) **515**, 237 (2014).

[46] A. Eckardt, Rev. Mod. Phys. **89**, 011004 (2017).

[47] S. A. Sato, J. W. McIver, M. Nuske, P. Tang, G. Jotzu, B. Schulte, H. Hübener, U. De Giovannini, L. Mathey, M. A. Sentef, A. Cavalleri, and A. Rubio, Phys. Rev. B **99**, 214302 (2019); J. W. McIver, B. Schulte, F.-U. Stein, T. Matsuyama1, G. Jotzu, G. Meier, and A. Cavalleri, Nat. Phys. **16**, 38 (2020).

[48] F. Meinert, M. J. Mark, K. Lauber, A. J. Daley, and H.-C. Nägerl, Phys. Rev. Lett. **116**, 205301 (2016).

[49] P. Bordia, H. P. Lüschen, S. S. Hodgman, M. Schreiber, I. Bloch, and U. Schneider, Phys. Rev. Lett. **116**, 140401 (2016); P. Bordia, H. Lüschen, U. Schneider, M. Knap, and I. Bloch, Nat. Phys. **13**, 460 (2017).

[50] S. Mukherjee, M. Valiente, N. Goldman, A. Spracklen, E. Andersson, P. Ohberg, and R. R. Thomson, Phys. Rev. A **94**, 053853 (2016).

[51] S. Blanes, F. Casas, J. A. Oteo, and J. Ros, Phys. Rep. **470**, 151 (2009).

[52] S. N. Shevchenko, S. Ashhab, and F. Nori, Phys. Rep. **492**, 1 (2010).

[53] L. D'Alessio and A. Polkovnikov, Ann. Phys. **333**, 19 (2013).

[54] M. Bukov, L. D'Alessio, and A. Polkovnikov, Adv. Phys. **64**, 139 (2015).

[55] L. D'Alessio, Y. Kafri, A. Polkovnikov, and M. Rigol, Adv. Phys. **65**, 239 (2016).

[56] T. Oka and S. Kitamura, Annu. Rev. Condens. Matter Phys. **10**, 387 (2019).

[57] S. Bandyopadhyay, S. Bhattacharjee, and D. Sen, J. Phys.: Condens. Matter **33**, 393001 (2021); A. Sen, D. Sen, and K. Sengupta, *ibid.* **33**, 443003 (2021).

[58] T. Oka and H. Aoki, Phys. Rev. B **79**, 081406(R) (2009); T. Kitagawa, T. Oka, A. Brataas, L. Fu, and E. Demler, *ibid.* **84**, 235108 (2011).

[59] T. Kitagawa, E. Berg, M. Rudner, and E. Demler, Phys. Rev. B **82**, 235114 (2010).

[60] N. H. Lindner, G. Refael, and V. Galitski, Nat. Phys. **7**, 490 (2011).

[61] L. Jiang, T. Kitagawa, J. Alicea, A. R. Akhmerov, D. Pekker, G. Refael, J. I. Cirac, E. Demler, M. D. Lukin, and P. Zoller, Phys. Rev. Lett. **106**, 220402 (2011).

[62] Z. Gu, H. A. Fertig, D. P. Arovas, and A. Auerbach, Phys. Rev. Lett. **107**, 216601 (2011).

[63] M. Trif and Y. Tserkovnyak, Phys. Rev. Lett. **109**, 257002 (2012).

[64] A. Gomez-Leon and G. Platero, Phys. Rev. B **86**, 115318 (2012); Phys. Rev. Lett. **110**, 200403 (2013).

[65] B. Dóra, J. Cayssol, F. Simon, and R. Moessner, Phys. Rev. Lett. **108**, 056602 (2012); J. Cayssol, B. Dóra, F. Simon, and R. Moessner, Phys. Status Solidi (RRL) **7**, 101 (2013).

[66] D. E. Liu, A. Levchenko, and H. U. Baranger, Phys. Rev. Lett. **111**, 047002 (2013).

[67] Q.-J. Tong, J.-H. An, J. Gong, H.-G. Luo, and C. H. Oh, Phys. Rev. B **87**, 201109(R) (2013).

[68] M. S. Rudner, N. H. Lindner, E. Berg, and M. Levin, Phys. Rev. X **3**, 031005 (2013); F. Nathan and M. S. Rudner, New J. Phys. **17**, 125014 (2015).

[69] Y. T. Katan and D. Podolsky, Phys. Rev. Lett. **110**, 016802 (2013).

[70] N. H. Lindner, D. L. Bergman, G. Refael, and V. Galitski, Phys. Rev. B **87**, 235131 (2013).

[71] A. Kundu and B. Seradjeh, Phys. Rev. Lett. **111**, 136402 (2013); A. Kundu, H. A. Fertig, and B. Seradjeh, *ibid.* **113**, 236803 (2014).

[72] T. L. Schmidt, A. Nunnenkamp, and C. Bruder, New J. Phys. **15**, 025043 (2013).

[73] A. A. Reynoso and D. Frustaglia, Phys. Rev. B **87**, 115420 (2013).

[74] C.-C. Wu, J. Sun, F.-J. Huang, Y.-D. Li, and W.-M. Liu, Europhys. Lett. **104**, 27004 (2013).

[75] M. Thakurathi, A. A. Patel, D. Sen, and A. Dutta, Phys. Rev. B **88**, 155133 (2013); M. Thakurathi, K. Sengupta, and D. Sen, *ibid.* **89**, 235434 (2014).

[76] P. M. Perez-Piskunow, G. Usaj, C. A. Balseiro, and L. E. F. Foa Torres, Phys. Rev. B **89**, 121401(R) (2014); G. Usaj, P. M. Perez-Piskunow, L. E. F. Foa Torres, and C. A. Balseiro, *ibid.* **90**, 115423 (2014); P. M. Perez-Piskunow, L. E. F. Foa Torres, and G. Usaj, Phys. Rev. A **91**, 043625 (2015).

[77] M. D. Reichl and E. J. Mueller, Phys. Rev. A **89**, 063628 (2014).

[78] D. Carpentier, P. Delplace, M. Fruchart, and K. Gawedzki, Phys. Rev. Lett. **114**, 106806 (2015).

[79] T.-S. Xiong, J. Gong, and J.-H. An, Phys. Rev. B **93**, 184306 (2016).

[80] C. Dutreix, E. A. Stepanov, and M. I. Katsnelson, Phys. Rev. B **93**, 241404(R) (2016).

[81] M. Thakurathi, D. Loss, and J. Klinovaja, Phys. Rev. B **95**, 155407 (2017).

[82] L. Zhou and J. Gong, Phys. Rev. B **97**, 245430 (2018).

[83] O. Deb and D. Sen, Phys. Rev. B **95**, 144311 (2017); S. Saha, S. N. Sivarajan, and D. Sen, *ibid.* **95**, 174306 (2017).

[84] S. Sur and D. Sen, Phys. Rev. B **103**, 085417 (2021).

[85] J. Zhang, P. W. Hess, A. Kyprianidis, P. Becker, A. Lee, J. Smith, G. Pagano, I.-D. Potirniche, A. C. Potter, A. Vishwanath, N. Y. Yao, and C. Monroe, Nature (London) **543**, 217 (2017).

[86] R. Peierls, Zeitschrift für Physik **80**, 763 (1933).

[87] M. Q. Weng, D. N. Sheng, Z. Y. Weng, and R. J. Bursill, Phys. Rev. B **74**, 012407 (2006).

[88] S. Yunoki and S. Sorella, Phys. Rev. B **74**, 014408 (2006).

[89] P. Hauke, Phys. Rev. B **87**, 014415 (2013).

[90] M. G. Gonzalez, B. Bernu, L. Pierre, and L. Messio, arXiv:2112.08128.

[91] A. Wietek and A. M. Läuchli, Phys. Rev. B **95**, 035141 (2017).

[92] S.-S. Gong, W. Zhu, J.-X. Zhu, D. N. Sheng, and K. Yang, Phys. Rev. B **96**, 075116 (2017).

[93] M. M. Rams and B. Damski, Phys. Rev. A **84**, 032324 (2011).

[94] M. Claassen, H.-C. Jiang, B. Moritz, and T. P. Devereaux, Nat. Commun. **8**, 1192 (2017).

[95] S. Kitamura, T. Oka, and H. Aoki, Phys. Rev. B **96**, 014406 (2017).

[96] E. V. Boström, M. Claassen, J. W. McIver, G. Jotzu, A. Rubio, and M. A. Sentef, SciPost Phys. **9**, 061 (2020).

[97] D. Sen and R. Chitra, Phys. Rev. B **51**, 1922 (1995).

[98] P. W. Anderson, Phys. Rev. **86**, 694 (1952).

[99] R. Kubo, Phys. Rev. **87**, 568 (1952).

[100] T. Holstein and H. Primakoff, Phys. Rev. **58**, 1098 (1940).

[101] W.-L. You, Y.-W. Li, and S.-J. Gu, Phys. Rev. E **76**, 022101 (2007).

[102] L. Wang, Y.-H. Liu, J. Imriška, P. N. Ma, and M. Troyer, Phys. Rev. X **5**, 031007 (2015).

[103] A. de la Torre, D. M. Kennes, M. Claassen, S. Gerber, J. W. McIver, and M. A. Sentef, Rev. Mod. Phys. **93**, 041002 (2021).

[104] V. L. Quito and R. Flint, Phys. Rev. Lett. **126**, 177201 (2021).

[105] V. L. Quito and R. Flint, Phys. Rev. B **103**, 134435 (2021).

[106] D. A. Abanin, W. De Roeck, and F. Huveneers, Phys. Rev. Lett. **115**, 256803 (2015).

[107] T. Mori, T. Kuwahara, and K. Saito, Phys. Rev. Lett. **116**, 120401 (2016).

[108] M. C. Tran, A. Ehrenberg, A. Y. Guo, P. Titum, D. A. Abanin, and A. V. Gorshkov, Phys. Rev. A **100**, 052103 (2019).

[109] T. Shirai, T. Mori, and S. Miyashita, Phys. Rev. E **91**, 030101(R) (2015).

[110] T. Shirai, J. Thingna, T. Mori, S. Denisov, P. Hänggi, and S. Miyashita, New J. Phys. **18**, 053008 (2016).

[111] J. Struck, C. Ölschläger, R. Le Targat, P. Soltan-Panahi, A. Eckardt, M. Lewenstein, P. Windpassinger, and K. Sengstock, Science **333**, 996 (2011).

[112] L. A. Eckardt, P. Hauke, P. Soltan-Panahi, C. Becker, K. Sengstock, and M. Lewensteinet, Europhys. Lett. **89**, 10010 (2010).

[113] E. P. Scriven and B. J. Powell, Phys. Rev. Lett. **109**, 097206 (2012).

[114] K. Yoshimi, H. Seo, S. Ishibashi, and S. E. Brown, Phys. B: Condens. Matter **407**, 1783 (2012).

[115] A. A. Tsirlin, A. Möller, B. Lorenz, Y. Skourski, and H. Rosner, Phys. Rev. B **85**, 014401 (2012).

[116] P. Weinberg and M. Bukov, SciPost Phys. **2**, 003 (2017); **7**, 020 (2019).